効率的な siRNA 送達システムの開発を目的とした
機能性脂質ナノ粒子の設計

Design of functional lipid nanoparticles
for development of an efficient siRNA delivery system

本論文は静岡県立大学大学院　博士論文である

2018 年 3 月

March 2018

静岡県立大学大学院　薬食生命科学総合学府

薬学専攻　博士課程　医薬生命化学講座

岡本　彩香

Ayaka Okamoto

Abbreviation

αHB-EGF LNP-siRNA: anti-HB-EGF Fab'-modified lipid nanoparticles encapsulating siRNA
BCA: bicinchoninic acid
BSA: bovine serum albumin
CPP: cell-penetrating peptide
Cho: cholesterol
Control LNP-siRNA: Mouse Fab'-modified lipid nanoparticles encapsulating siRNA
DAPI: 4',6-diamidino-2-phenylindole
DETA: diethylenetriamine
DIC: differential interference contrast
DiO: 3,3'-dioctadecyloxacarbocyanine perchlorate
DDS: drug delivery system
DEPC: diethylpyrocarbonate
DMPG: dimyristoylphosphatidylglycerol
DOPE: dioleoylphosphatidylethanolamine
DPPC: dipalmitoylphosphatidylcholine
DSPE: distearoylphosphatidylethanolamine
ECL: enhanced chemiluminescence
EDA: ethylenediamine
EPR: enhanced permeability and retention
ER: estrogen receptor
FITC: fluorescein isothiocyanate
FBS: fetal bovine serum
HB-EGF: heparin-binding epidermal growth factor-like growth factor
HER2: human epidermal growth factor receptor 2
HRP: horseradish peroxidase
ITC: ithothermal titration calorimetry
LNP: lipid nanoparticles
LVs: lipid vesicles
mal: maleimide
PAGE: polyacrylamide gel electrophoresis
PBS: phosphate-buffered saline
PEG: polyethylene glycol
PMSF: phenylmethylsulfonyl fluoride
PP-13: palmitoyl protamine-13
PR: progesterone receptor
PVDF: polyvinylidine difluoride
RISC: RNA-induced silencing complex
RNAi: RNA interference
RT-PCR: reverse transcription-polymerase chain reaction
SDS: sodium dodecyl sulfate
siRNA: small interfering RNA
TNS: 6-(*p*-toluidino)-2-naphthalenesul-fonic acid

Chemical structures of lipids

Cholesterol (M.W. =386.65)

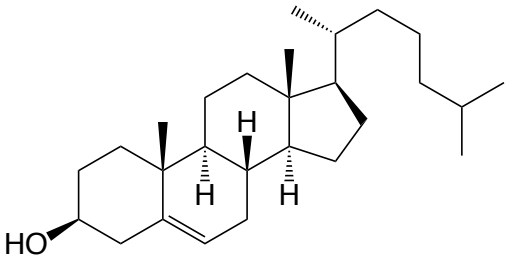

Dimyristoylphosphatidylglycerol (DMPG, M.W. = 688.85)

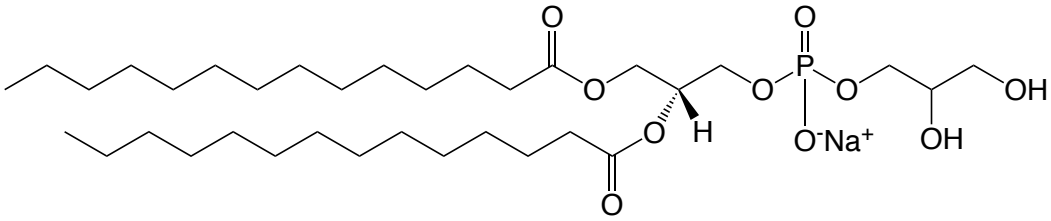

Dioleoylphosphatidylethanolamine (DOPE, M.W. = 744.03)

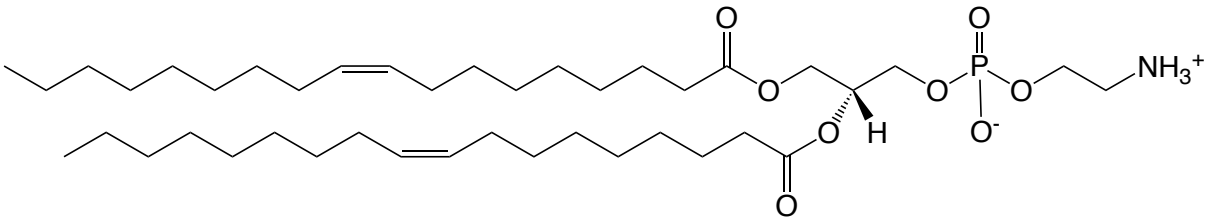

Dipalmitoylphosphatidylcholine (DPPC, M.W. = 734.04)

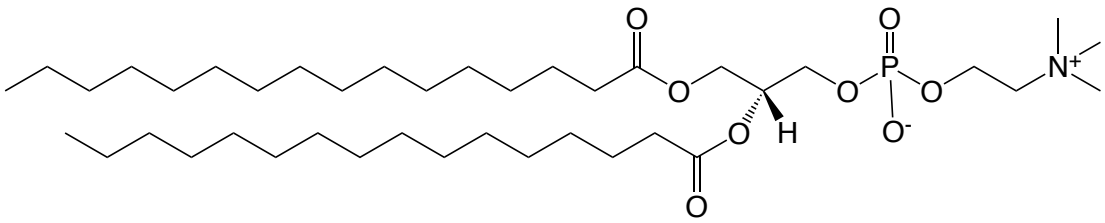

Dicetylphosphate-ethylendiamine-CH_2R conjugate (DCP-EDA-CH_2R)
(R indicates: -CH_3, M.W. 617.00; -CH_2F, M.W. 634.99; -CHF_2, M.W. 652.98; -CF_3, M.W. 670.97)

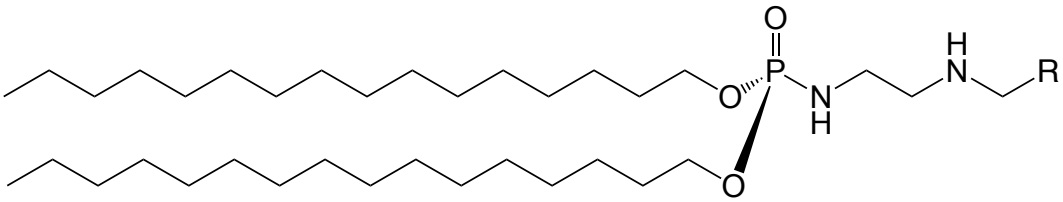

Dicetylphosphate-diethylentriamine-CH_2R conjugate (DCP-DETA-CH_2R)
(R indicates: -CH_3, M.W. 660.07; -CH_2F, M.W. 678.06; -CHF_2, M.W. 696.05; -CF_3, M.W. 714.04)

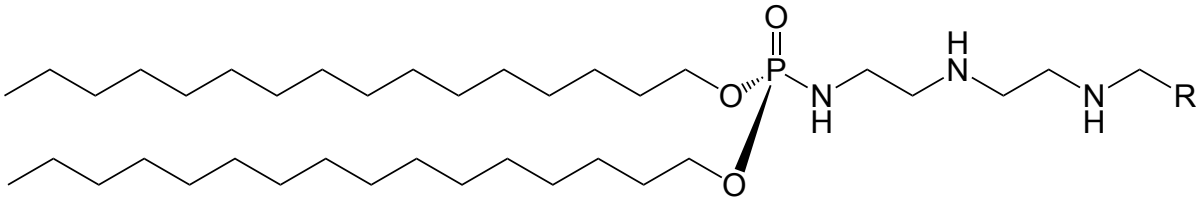

Contents

Foreword

Small-molecular and biological drugs have made significant contributions in curing diseases. However, there are a lot of undruggable target proteins that lack a drug-accessible compartment. In addition, problems such as the limitation of applicable patients due to their gene profiles or disease situation are still unsolved. Small interfering RNA (siRNA) has received considerable attention as a therapeutic candidate capable of overcoming these problems.

siRNA is a double-stranded RNA having 21 to 23 base pairs, which guides RNA-induced silencing complex (RISC) to target mRNA with sequence-dependent high selectivity and leads to cleavage of mRNA by argonaute2[1,2]. As siRNA can be designed based on target mRNA sequence and synthesized by chemical synthesis, it has been considered as drug candidates to address unmet medical needs. However, it is well known both that siRNA is likely to be eliminated from the blood (halflife = 1.8 min[3]) by rapid degradation and glomerular filtration through the kidneys, and that siRNA has difficulty in penetrating cell membranes[4]. Therefore, an appropriate siRNA delivery system is necessary for the establishment of siRNA therapies. For this purpose, nanoparticle-mediated delivery of siRNA has been studied to obtain efficient gene silencing[5-7].

In the most advanced clinical development, European Medicines Agency (EMA) granted priority review for the application of Patisiran developed by Alnylam in November 2017. Patisiran is siRNA-containing lipid nanoparticle for patients with hereditary transthyretin amyloidosis (hATTR)[8]. Furthermore, lipid nanoparticles such as liposomes are the most often used as carriers in clinical trials of siRNA conducted in the world[9]. These data suggest that lipid nanoparticles are quite actively studied carriers in siRNA delivery.

In this thesis, I describe two studies on siRNA delivery using lipid nanoparticles. In Part 1, I describe the development of antibody-modified lipid nanoparticles encapsulating siRNA for the treatment of triple-negative breast cancer for which there is no effective therapeutic agent. In the second part, for the purpose of constructing an siRNA vector design strategy to achieve effective RNA interference, the effect of pK_a of cationic lipid precisely controlled by fluorine atom on siRNA delivery was investigated.

Part 1. siRNA delivery using anti-HB-EGF antibody-modified lipid nanoparticles for the treatment of triple-negative breast cancer

Part 1. - Introduction

Among WHO member countries, the Japan has the longest life expectancy in the world[10]. This situation has been attributed to the high-quality food, highly-developed economy, and advanced medical care present in Japan. On the other hand, mortality due to cancer and heart disease and pneumonia still continues to rise. Especially cancer is the leading cause of death in our country[11], and development of an effective remedy for improving the quality of life (QOL) of patients is desired. Triple-negative breast cancer (TNBC) is known as a refractory cancer because it does not express drug target genes, such as estrogen receptors (ER), progesterone receptors (PR), or human epidermal growth factor receptor 2 (HER2)[12]. As TNBC accounts for about 15% of breast cancers and tends to have high malignancy and poor prognosis[13], the development of a novel TNBC therapeutic strategy is urgently required, and many studies of RNA interference-based therapy with siRNA have been reported. Several studies have used siRNA-delivery systems to treat TNBC, including cyclodextrin-grafted polyethylenimine (PEI) functionalized mesoporous silica nanoparticles[14], siRNA conjugated to a diacyl lipid moiety[15], PEI substituted with linoleic acid[16], chitosan-gold nanorods[17], cationic lipid assisted poly(ethylene glycol)-*b*-poly(D,L-lactide) (PEG-PLA) nanoparticles[18], and (1-aminoethyl)iminobis[*N*-oleicylsteinyl-1-aminoethyl]propionamide] (ECO)-based lipid nanoparticles[19]. These reports indicate that RNA interference by siRNA has potential as an innovative therapeutic strategy for TNBC, if an appropriate carrier can be developed. While a variety of technologies are available for the passive-targeting of siRNA to TNBC, until now there has been no system for the active-targeting of specific tumors.

Here, lipid nanoparticles have been developed for TNBC treatment that encapsulate siRNA modified with an antibody targeting heparin-binding epidermal growth factor-like growth factor (HB-EGF). HB-EGF is a ligand that binds to the EGF receptor (EGFR) and is related to various physiological and pathological functions, such as heart development[20], perinatal distal lung development[21], and wound healing[22]. In addition, HB-EGF is known to be highly expressed on the surface of various cancers, including breast, ovarian, and gastric cancer[23]. HB-EGF is highly likely to be involved in tumor progression by activating the signaling pathway for tumorigenesis[24], promoting angiogenesis[25], and increasing tumor metastasis[26]. In TNBC patients, HB-EGF has been reported to show high expression level among the EGFR ligands, which also include amphiregulin, transforming growth factor-α (TGFα), and EGF[27]. It has been investigated as target molecules of particular tumors. For example, CRM197, which is a mutant of diphtheria toxin, has been used as an HB-EGF inhibitor for the treatment of breast cancer[27,28]. The C-terminal receptor domain of the diphtheria toxin has been coated on poly(lactic-*co*-glycolic acid) nanoparticles to target HB-EGF-expressing glioblastoma[29]. These reports suggest that HB-EGF is very likely to be useful as an address-molecule for tumor targeting.

In this study, lipid nanoparticles (LNP) encapsulating siRNA (LNP-siRNA) were designed, and modified with Fab' fragment of anti-HB-EGF antibody (αHB-EGF LNP-siRNA, **Scheme 1**) for treatment of TNBC. In Chapter 1, the ability of αHB-EGF LNP-siRNA to enter MDA-MB-231 human TNBC cells, which express HB-EGF on its cell surface, and to induce RNA interference activity *in vitro* was evaluated using siRNA against polo-like kinase 1 (siPLK1). PLK1 is a protein that is related to the cell cycle, and is reported that its knockdown results in apoptotic cell death[30]. In particular, inhibition of PLK1 is known to cause synthetic lethality in Kras-mutant cells[31] such as MDA-MB-231. So, it was hypothesized that PLK1 knockdown would result in the suppression of MDA-MB-231 growth

effectively. In Chapter 2, I evaluated the potentials of αHB-EGF LNP as a siRNA vector *in vivo* were examined. αHB-EGF LNP-siPLK1 was administered to MDA-MB-231 carcinoma-bearing mice, and its utility as a candidate for TNBC treatment was evaluated.

Scheme 1. Schematic image of cytoplasmic siRNA delivery using anti-HB-EGF LNP-siRNA via the HB-EGF expressed on the cell surface

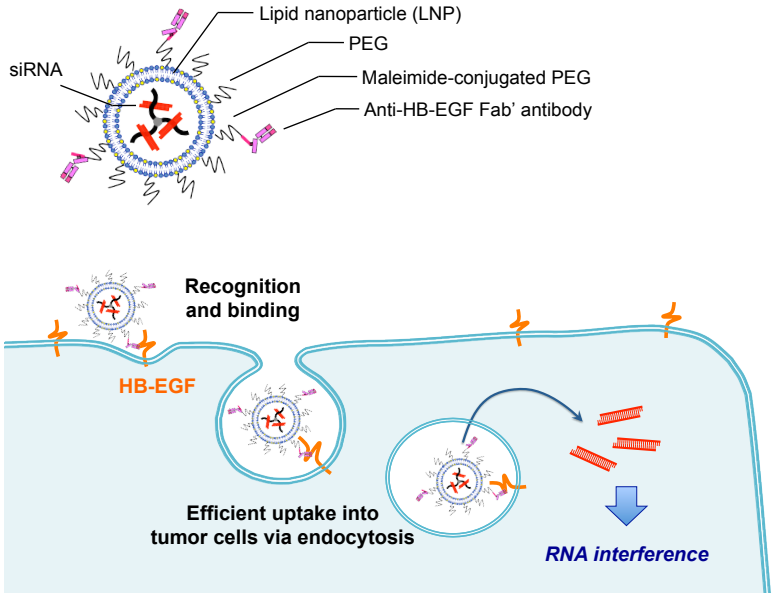

[Chapter 1.] siRNA delivery to MDA-MB-231 human TNBC cells using anti-HB-EGF antibody-modified lipid nanoparticles.

Active targeting of nanoparticles to tumors by antibody conjugation is a promising approach, since tumor cells often express characteristic molecules on their surface that are not found on normal cells[32,33]. HB-EGF is known to highly express on the cell surface of various cancers. The precursor of HB-EGF is expressed on the cell surface as a membrane-anchored form (proHB-EGF) and then processed to a soluble form (HB-EGF), which mediates the intracellular signaling. Hence, I expected HB-EGF to be a useful target molecule for delivering siRNA to tumors. Here, LNP-siRNA modified with Fab' fragments of anti-HB-EGF antibody (αHB-EGF LNP-siRNA) was developed, and evaluated their potential as a siRNA vector *in vitro*.

1-[1]-1. Experimental Section

1-[1]-1-1. Materials

siRNA against luciferase 2 (siLuc2) and against polo-like kinase 1 (siPLK1) were purchased from Hokkaido System Science Co. (Hokkaido, Japan). In this study, siLuc2 was used as a control siRNA (siCont). The nucleotide sequences with a 2-nucleotide overhang (underline) for siLuc2 were 5'-GCU AUG GGC UGA AUA CAA ATT-3' (passenger) and 5'-UUU GUA UUC AGC CCA UAG CTT-3' (guide), and for siPLK1 were 5'-CAA CAC GCC UCA UCC UCU ATT-3' (passenger) and 5'-UAG AGG AUG AGG CGU GUU GTT-3' (guide). For the use of fluorescein isothiocyanate (FITC)-labeled siRNA, FITC was conjugated to siLuc2 at the 3' end of the guide strand. A palmitoyl conjugate of

protamine-derived 13-amino-acid peptide (PP-13) was purchased from Operon Biotechnologies (Tokyo, Japan). The amino acid sequence of PP-13 was RRRRRRGGRRRRG(Lys[Palmitoyl])-NH_2. Dimyristoylphosphoglycerol (DMPG), distearoylphosphatidylethanolamine-polyethyleneglycol (DSPE-PEG) 5000, and maleimide-conjugated DSPE-PEG5000 (DSPE-PEG-maleimide) were purchased from NOF Co. (Tokyo, Japan). Dioleoylphosphatidylethanolamine (DOPE) and cholesterol were kindly provided by Nippon Fine Chemical Co. (Hyogo, Japan). Monoclonal antibody clone 3E9 specific for human HB-EGF was obtained by a method described previously[34]. Pepsin from porcine gastric mucosa was purchased from Merck KGaA (Darmstadt, Germany). Primers of PLK1 and β-actin were purchased from Rikaken Co. Ltd. (Aichi, Japan). The nucleotide sequences of the primers of PLK1 were 5'-CAC AGT GTC AAT GCC TCC AA-3' (forward) and 5'-TTG CTG ACC CAG AAG ATG G-3' (reverse), and those of β-actin, 5'-CAT CCG TAA AGA CCT CTA TGC CAA C-3' (forward) and 5'-ATG GAG CCA CCG ATC CAC A-3' (reverse). Anti-PLK1 rabbit polyclonal antibody and anti-β-actin rabbit polyclonal antibody were purchased from Cell Signaling Technology (MA, USA) and Novus Biologicals (CO, USA), respectively. Horseradish peroxidase (HRP)-conjugated anti-rabbit immunoglobulin G (IgG) polyclonal antibody was purchased from GE Healthcare (Little Chalfont, UK).

1-[1]-1-2. Preparation of lipid nanoparticles encapsulating siRNA (LNP-siRNA)

siRNA and PP-13 (1/16.8 as a molar ratio, containing 1 nmol of siRNA) dissolved in RNase-free water (1 mL, Invitrogen, Rockville, MD) were mixed and incubated for 30 min at room temperature to obtain the cationic core. DOPE, cholesterol, and DMPG (6/5/2 as a molar ratio, total lipids: 5 μmol) dissolved in chloroform were evaporated under reduced pressure, and stored *in vacuo* for at least 1 h. LNP-siRNA was prepared by hydration of the

thin lipid film with 1 mL of the cationic core solution and sized by use of mild sonication for 3 min at room temperature. The particle size and ζ-potential of the particles in 10 mM phosphate buffer (pH 7.4) were measured using a Zetasizer Nano ZS (Malvern, Worcs, UK).

1-[1]-1-3. Preparation of anti-HB-EGF Fab' flagment

Fab' fragments of anti-HB-EGF monoclonal antibody were prepared as described previously[35]. Digestion of anti-HB-EGF monoclonal IgG with pepsin was performed in 100 mM sodium citrate buffer (pH 3.5). Pepsin was added to the IgG solution at a final enzyme / IgG ratio of 4 w/w%. The mixture was incubated for 3 h at 37°C to eliminate the Fc region of the IgG. The reaction was terminated by addition of a 10% volume of 3 M Tris-HCl (pH 7.5). The generated $F(ab')_2$ fragment was washed and concentrated by ultrafiltration (5,000 ×*g*, 20 min, 4°C) using an Amicon® Ultra-4 (10,000 NMWL, Merck KGaA) in 100 mM sodium phosphate buffer (pH 6.8). To obtain anti-HB-EGF Fab', the $F(ab')_2$ was reduced with cysteamine hydrochloride (final concentration: 10 mM) for 1.5 h at 37°C. Then, the Fab' fraction was purified by gel-filtration chromatography (1.0 cm × 45 cm, Ultrogel® AcA 54, Merck), and concentrated by ultrafiltration (5,000 ×*g*, 20 min, 4°C) using Amicon® Ultra-4 (10,000 NMWL).

1-[1]-1-4. Modification of anti-HB-EGF Fab' flagment to the surface of LNP-siRNA

For the modification of LNP-siRNA with Fab' fragments of anti-HB-EGF antibody, 1 mL of the LNP-siRNA solution was incubated with 45 μL of 5 mM DSPE-PEG and 5 μL of 5 mM DSPE-PEG-maleimide dissolved in RNase-free water at 37°C for 2 h, forming PEG/PEG-maleimide-inserted LNP-siRNA (PEG-mal-LNP-siRNA). The Fab' fragments and PEG-mal-LNP-siRNA (1/1 as a molar ratio of Fab' and maleimide moiety) were mixed, and the coupling reaction was carried out at 4°C for 16 h. After ultracentrifugation (453,000 ×*g*,

4°C, 15 min), anti-HB-EGF Fab'-modified LNP (αHB-EGF LNP-siRNA) was re-suspended with RNase-free water. Similarly, the surface of LNP-siRNA was decorated with Fab' fragments of control mouse IgG (MGG-0500, MBL, Nagoya, Japan; Control LNP-siRNA). The particle size and ζ-potential of the particles in 10 mM phosphate buffer (pH 7.4) were measured using a Zetasizer Nano ZS (Malvern). The amount of Fab' antibody modified on LNP-siRNA was measured using high-performance liquid chromatography (Hitachi High-Tech Science Corporation, Tokyo, Japan). Control LNP-siRNA and αHB-EGF LNP-siRNA were solubilized with 2% sodium dodecyl sulfate (SDS, Wako Pure Chemical Industries, Ltd., Osaka, Japan), and subjected to a column of TSKgel G3000SW_{XL} (Tosoh Bioscience LLC, PA, USA) with flow rate of 0.5 mL/min (30 min, 30°C). Mobile phase was composed of 0.1% SDS, 0.1 M NaH_2PO_4, 0.1 M Na_2SO_4. pH of the mobile phase was adjusted to 6.7 with NaOH. Fab' was detected using UV Detercter L-2400 (Hitachi High-Tech Science Corporation).

1-[1]-1-5. Cell culture

MDA-MB-231 human triple-negative (ER-, PR- and HER2-negative) breast cancer cells were purchased from ATCC (Manassas, VA). Overexpression of HB-EGF in MDA-MB-231 triple-negative breast cancer cells was already demonstrated in previous study[35]. The cells were cultured in RPMI-1640 medium (Wako Pure Chemical Industries, Ltd., Osaka, Japan) supplemented with 10% fetal bovine serum (FBS, AusGeneX, Oxenford, Australia), 100-units/mL penicillin G (MP Biomedicals, Irvine, CA), and 100-μg/mL streptomycin (MP Biomedicals) in a CO_2 incubator.

1-[1]-1-6. siRNA transfection

MDA-MB-231 cells were seeded onto a culture plate and pre-cultured overnight. The

medium was changed to a fresh one containing FBS but not antibiotics before transfection. Control LNP-siRNA or αHB-EGF LNP-siRNA was added to the culture medium at a final concentration of 100 nM (as siRNA), and the cells were then incubated for 24 h at 37°C in a 5% CO_2 incubator. After a medium change, the cells were incubated for the desired time as described for each experimental procedure.

1-[1]-1-7. Association of αHB-EGF LNP-siRNA with MDA-MB-231 cells

MDA-MB-231 cells (4×10^4 cells/0.5 mL/well) were seeded onto 24-well plates (BD Bioscience, San Jose, CA). These cells were incubated for 6, 12 or 24 h with FITC-labeled siRNA (60 nM) formulated in Control LNP or αHB-EGF LNP. Naked FITC-siRNA was also incubated with the cells as a control. The cells were washed 3 times with PBS and lysed with 1 w/v% *n*-octyl-*β*-D-glucoside (Dojindo, Kumamoto, Japan) containing protease inhibitors (1 mM phenylmethylsulfonyl fluoride; PMSF, 2 μg/mL aprotinin, 2 μg/mL leupeptin, and 2 μg/mL pepstatin A). The fluorescence intensity of FITC was determined with a Tecan Infinite M200 microplate reader (Salzburg, Austria) according to the manufacturer's instructions (ex. 495 nm, em. 535 nm) and corrected by total protein content measured with a Pierce™ BCA Protein Assay Kit (Thermo Fisher Scientific Inc., Kanagawa, Japan) according to the manufacturer's instructions.

1-[1]-1-8. Cellular uptake of αHB-EGF LNP into MDA-MB-231 cells

MDA-MB-231 cells were seeded onto 8-well chamber slides (Thermo Fisher Scientific) at a density of 1×10^4 cells/well and incubated with FITC-labeled siRNA alone (naked siRNA), Control LNP-siRNA or αHB-EGF LNP-siRNA (60 nM as siRNA) for 24 h. After having been washed with PBS containing 30-units/mL heparin (Mochida Pharmaceutical Co., Ltd., Tokyo, Japan), the cells were fixed with 4% paraformaldehyde for

30 min; and the nuclei were then stained with 4',6-diamidino-2-phenylindole (DAPI, Life Technologies, Carlsbad, CA, USA). Intracellular localization of siRNA was observed by using confocal laser-scanning microscopy (LSM510 META, Carl Zeiss, Germany). For evaluation of intracellular distribution of FITC-siRNA formulated in αHB-EGF LNP, lysosome was stained with Lysotracker (Thermo Fisher Scientific) before the fixation.

1-[1]-1-9. Suppression of PLK1 mRNA expression

MDA-MB-231 cells were seeded onto a 6-well plate at a density of 1×10^5 cells / 2 mL and incubated overnight. The medium was changed to a fresh one containing FBS but not antibiotics before transfection. The cells were transfected with αHB-EGF LNP-siCont, Control LNP-siPLK1, or αHB-EGF LNP-siPLK1 at a final concentration of 100 nM as siRNA, and then incubated for 24 h. According to the manufacturer's protocol, the total RNA of the cells was extracted with TRIzol LS reagent (Thermo Fisher Scientific Inc.). One microgram of total RNA was applied to the synthesis of complementary DNA with a First-Strand cDNA Synthesis Kit (GE Healthcare). In the presence of either human PLK1 primers or β-actin primers and SYBR Premix Ex Taq II (Takara Bio, Shiga, Japan), real-time RT-PCR was performed with a Thermal Cycler Dice Real Time System (Takara Bio). The conditions for PCR were as follows: 95°C for 30 sec (1 cycle), 95°C for 5 sec, 60°C for 30 sec (60 cycles).

1-[1]-1-10. Suppression of PLK1 protein expression

MDA-MB-231 cells were seeded onto a 6-well plate (5×10^4 cells / 2 mL) and pre-cultured overnight. After a medium change to a fresh one containing FBS but not antibiotics, the cells were transfected with αHB-EGF LNP-siCont, Control LNP-siPLK1, or αHB-EGF LNP-siPLK1 (100 nM as siRNA). After 24 h, the medium was changed to a fresh

one containing FBS and antibiotics, and then the cells were cultured for an additional 48 h. The cells were washed with PBS and lysed with 0.1% SDS containing protease inhibitors (1 mM PMSF, 2 μg/mL aprotinin, 2 μg/mL leupeptin, and 2 μg/mL pepstatin A) in 150 mM NaCl / 10 mM Tris-HCl (pH 7.5). The cell lysate was applied for Western blotting.

1-[1]-1-11. Western blotting

Protein concentration was measured by bicinchoninic acid (BCA) assay with a Pierce™ BCA Protein Assay Kit (Thermo Fisher Scientific Inc.). Cell lysates containing 10-μg protein were subjected to 10% SDS-PAGE and transferred electrophoretically to a polyvinylidene difluoride (PVDF) membrane (Millipore, Billerica, MA). After having been blocked for 1 h at 37°C with 5% bovine serum albumin (BSA, Sigma-Aldrich) in Tris-HCl-buffered saline containing 0.1% Tween 20 (TTBS, pH 7.4), the membrane was incubated with a primary antibody against PLK1 (1:1,000) or β-actin (1:5,000) overnight at 4°C, and then with an HRP-conjugated secondary antibody (1:10,000) for 1 h at room temperature. Each sample was developed by use of a chemiluminescent substrate (ECL-prime, GE Healthcare), and the chemiluminescence was detected with a LAS-3000 mini system (Fuji Film, Tokyo, Japan).

1-[1]-1-12. Growth inhibition assay

MDA-MB-231 cells were seeded onto a 96-well plate (Thermo Fisher Scientific Inc.) at a density of 2×10^3 cells/well with 180 μL of RPMI-1640 medium containing FBS but not antibiotics, and transfected with 20 μL of αHB-EGF LNP-siCont, Control LNP-siPLK1, or αHB-EGF LNP-siPLK1 (100 nM; 20 pmol/200 μL as siRNA) for 24 h. After a medium change, the cells were incubated for the desired time as described below. Cell viability was measured by WST-8 assay with a Cell Counting Kit-8 (Dojindo Laboratries, Kumamoto,

Japan) at 0, 1, 3, 5, and 7 days after transfection. In accordance with the manufacturer's protocol, WST-8 assay reagent (Cell Counting Kit-8 : medium = 1 : 9) was added after removing the culture media, and then the cells were incubated for 2 h at 37°C. To determine cell viability, absorbance at 450 nm was measured. In cases in which the cells were cultured for more than 3 days, the medium was changed to a fresh one containing FBS and antibiotics at day 4.

1-[1]-1-13. Statistical analysis

Differences within a group were evaluated by analysis of variance (ANOVA) with the Tukey *post-hoc* test.

1-[1]-2. Results

1-[1]-2-1. Characteristics of αHB-EGF LNP-siRNA

The physicochemical properties of each type of LNP-siRNA are shown in Table 1. LNP-siRNA had a particle size of 129 ± 30 nm and a ζ-potential of -45 ± 7.1 mV in 10 mM phosphate buffer (pH 7.4). On the other hand, αHB-EGF LNP-siRNA and Control LNP-siRNA both had a particle size of smaller than 200 nm and an almost neutral surface charge. The degree of modification of anti-HB-EGF Fab' antibody was about 130 μg Fab' / 1 μmol lipid.

Table 1. Characteristics of LNP-siRNA, PEG LNP-siRNA, Control LNP-siRNA, and αHB-EGF LNP-siRNA

	Size (d.nm)	PdI	ζ-Potential (mV)	Fab' conjugation (μg/μmol lipid)
LNP-siRNA	129 ± 30	0.242 ± 0.045	-45 ± 7.1	-
PEG LNP-siRNA	103 ± 15	0.265 ± 0.008	-2.8 ± 1.2	-
Control LNP-siRNA	138 ± 17	0.247 ± 0.047	-8.3 ± 3.9	126 ± 18
αHB-EGF LNP-siRNA	167 ± 56	0.284 ± 0.084	-5.9 ± 2.6	129 ± 14

1-[1]-2-2. Uptake of αHB-EGF LNP-siRNA into MDA-MB-231 cells

The association of αHB-EGF LNP-siRNA with MDA-MB-231 cells was examined by use of FITC-labeled siRNA. As shown in **Figure 1A**, αHB-EGF LNP-siRNA were significantly bound to the surface of the cells and/or taken up into the cells compared to the naked siRNA or Control LNP-siRNA. In addition, the amount of association increased in a time-dependent manner. Then, the intracellular distribution of FITC-siRNA in the transfected MDA-MB-231 cells was observed by confocal laser-scanning microscopy. As a result, FITC-siRNA delivered in the αHB-EGF LNP was homogeneously distributed throughout the cytoplasm of individual cells (**Figure. 1B**). In contrast, the fluorescence was quite weak or hardly observed when FITC-siRNA was delivered via the Control LNP-siRNA or applied in its naked form, respectively. FITC-siRNA and lysosome were separately localized in αHB-EGF LNP-siRNA-transfected cells (**Figure 1C**).

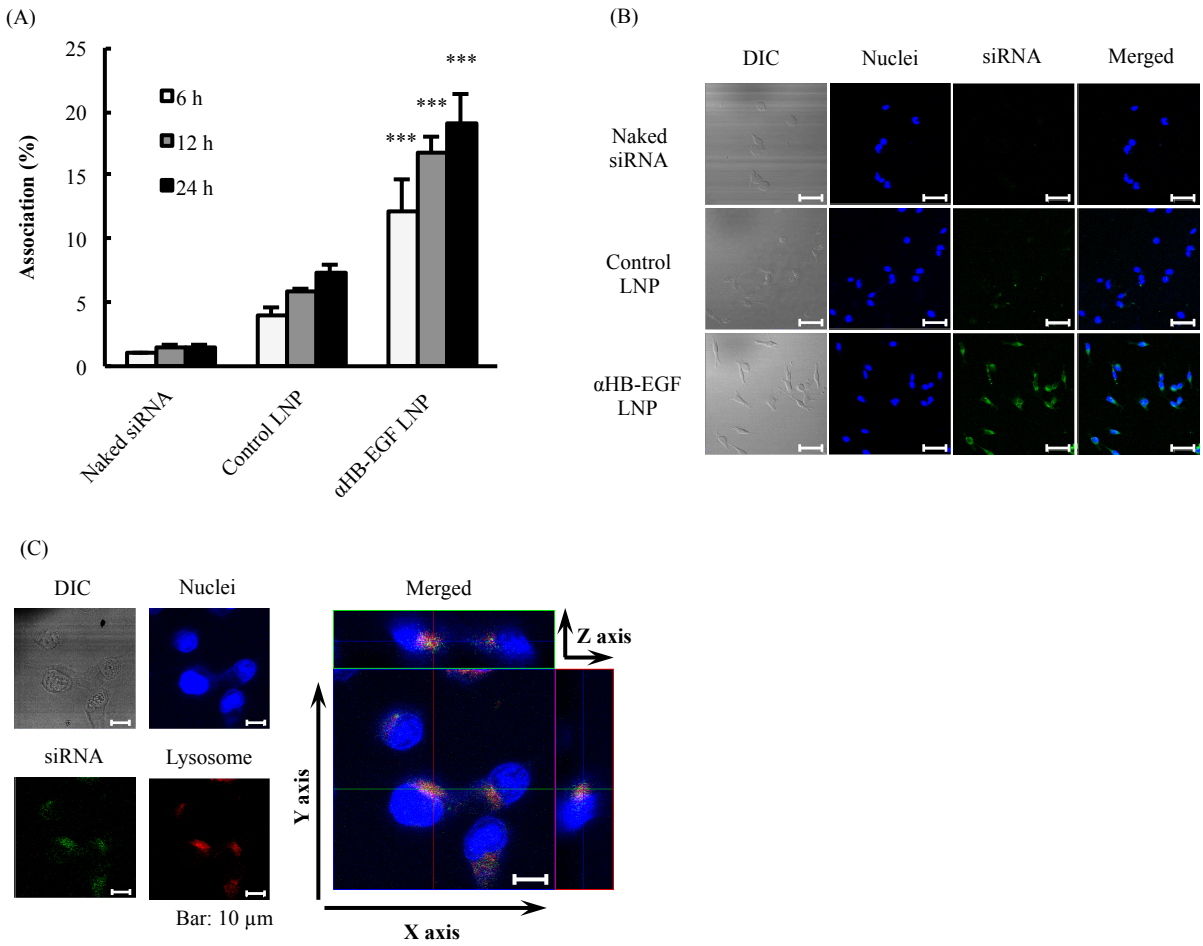

Figure 1. Uptake of αHB-EGF LNP-siRNA into MDA-MB-231 cells

(A) Association of αHB-EGF LNP-siRNA with MDA-MB-231 cells. Naked FITC-siRNA (Control) or FITC-siRNA formulated in Control LNP or αHB-EGF LNP was incubated with MDA-MB-231 cells for 6, 12 or 24 h at 37°C. After the cells had been lysed, the fluorescence intensity of the FITC-siRNA was determined. Data are presented as percentages (with SD bars) of siRNA detected in the cell lysate to that in the whole amount added. Asterisks indicate significant differences (***$P < 0.001$ *vs*. Control LNP-siRNA). (B) Intracellular distribution of siRNA in MDA-MB-231 cells that had been transfected with αHB-EGF LNP bearing FITC-labeled siRNA FITC-siRNA (green) taken up into the cells was observed by confocal laser-scanning microscopy. MDA-MB-231 cells were incubated with naked FITC-siRNA, Control LNP-FITC-siRNA, or αHB-EGF LNP-FITC-siRNA for 24 h at 37°C. The nuclei were stained with DAPI (blue). The scale bars indicate 50 μm. (C) Intracellular localization of siRNA in MDA-MB-231 cells. MDA-MB-231cells were transfected with αHB-EGF LNP-FITC-siRNA for 24 h. Lysosome were stained with Lysotracker (red). The scale bars indicate 10 μm.

1-[1]-2-3. Gene silencing effect of αHB-EGF LNP-siRNA

Gene silencing activity of αHB-EGF LNP-siPLK1 against MDA-MB-231 cells was determined. The relative amount of PLK1 mRNA in the cells was reduced by treatment with αHB-EGF LNP encapsulating siPLK1 (**Figure 2A**). More than 80% of PLK1 mRNA expression was suppressed by treatment with αHB-EGF LNP-siPLK1. Also, the amount of PLK1 mRNA in the Control LNP-siPLK1-treated cells was slightly reduced (approximately 24% reduction). In addition, PLK1 protein expression was clearly suppressed by treatment with αHB-EGF LNP-siPLK1 (**Figure 2B**). No silencing effects were observed in PLK1 mRNA or protein after treatment with αHB-EGF LNP-siCont. Furthermore, cell growth was inhibited after treatment with αHB-EGF LNP-siPLK1 (**Figure 2C**). At day 7, the αHB-EGF LNP-siPLK1-treated group showed about 45% inhibition compared with control (RNase-free water). On the other hand, Control LNP-siPLK1 and αHB-EGF LNP-siCont had no effect on cell growth.

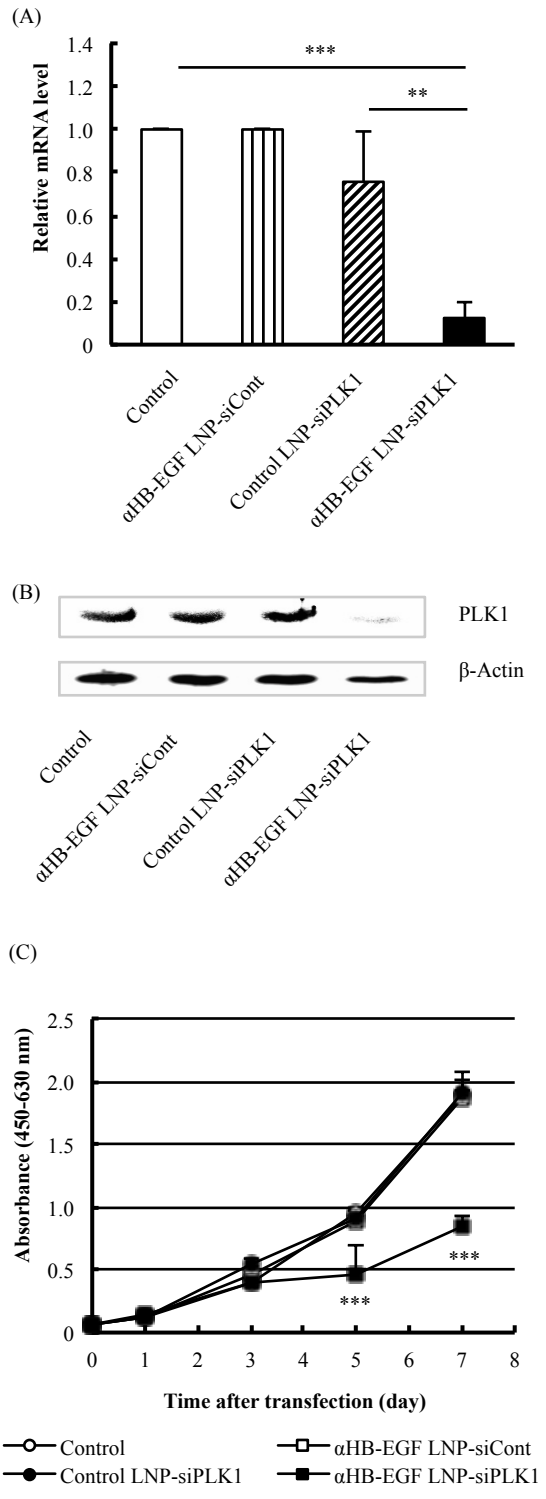

Figure 2. Gene silencing by siRNA formulated in αHB-EGF LNP. (A) Reduction of PLK1 mRNA in MDA-MB-231 cells after the treatment with αHB-EGF LNP-siPLK1. The cells were transfected for 24 h with siPLK1 encapsulated in Control LNP or αHB-EGF LNP. The expression of PLK1 mRNA was determined by real-time RT-PCR. Data are shown as relative expression level of PLK1 mRNA to that in the control (vehicle: RNase-free water) with SD bars. Asterisks indicate significant differences (***P<0.001, **P<0.01). (B) Knockdown of PLK1 protein by αHB-EGF LNP-siPLK1 in MDA-MB-231 cells. The cells were incubated with αHB-EGF LNP-siCont, Control LNP-siPLK1, or αHB-EGF LNP-siPLK1 for 24 h and cultured for an additional 48 h. The protein expression of PLK1 and β-actin was determined by Western blotting. (C) Inhibition of cell growth by the treatment with αHB-EGF LNP-siPLK1. MDA-MB-231 cells were treated with RNase-free water as control (○), αHB-EGF LNP-siCont (□), Control LNP-siPLK1 (●), or αHB-EGF LNP-siPLK1 (■) for 24 h. Viability of the cells was evaluated at 0, 1, 3, 5, or 7 days after the transfection by WST-8 assay. Symbol indicates a significant deference (***P<0.001 *vs.* control, αHB-EGF LNP-siCont, and Control LNP-siPLK1).

1-[1]-3. Discussion

Specific antibody is expected to have excellent characteristics for use in targeted delivery of siRNA for the following reasons: the specificity and binding affinity are considerably high[36]; internalization occurs via receptor-mediated endocytosis[37]; and practical utility is demonstrated in the clinical setting[38]. For these reasons, LNP modified with an antibody can be considered as a promising vector for delivering siRNA into the cytoplasm of target cells safely and specifically. In the present study, anti-HB-EGF Fab' antibody was conjugated to the LNP for targeted delivery of siRNA and evaluated selective gene silencing against MDA-MB-231 human triple-negative breast cancer (TNBC) cells.

Dynamic light scattering measurements showed that all of the particles had diameters between 100 and 200 nm. As it has previously been shown that particles with a size of less than 200 nm can be delivered to tumor tissue via the enhanced permeability and retention (EPR) effect[39], it is likely that αHB-EGF LNP-siRNA will be able to accumulate in tumor tissue in a similar manner. The ζ-potential data indicate that the surfaces of LNP-siRNA were effectively decorated with PEG or antibody-modified PEG, respectively. Because doxorubicin-encapsulating liposomes have their therapeutic effect enhanced with about 30 μg Fab' antibody / 1 μmol lipid[40], αHB-EGF LNP-siRNA is likely to be effective for ligand-mediated targeting to HB-EGF-expressing cells, including TNBCs although modification amount of Fab' was not optimized at present.

A ligand for the membrane-anchored form of HB-EGF has been reported to be internalized by ligand-mediated receptor endocytosis[41,42]. As expected, αHB-EGF LNP-siRNA were highly taken up into MDA-MB-231 cells which highly express HB-EGF (**Figure 1A**). Because siRNA was homogeneously distributed throughout the cytoplasm of the cells by delivery in αHB-EGF LNP (**Figure 1B**, **1C**), the endocytotic pathway via the

membrane-anchored form of HB-EGF might be useful for siRNA delivery.

Then, the utility of αHB-EGF LNP-siPLK1 was examined as an RNAi-based therapeutic agent *in vitro*. **Figure 2A** and **2B** showed that αHB-EGF LNP-siPLK1 induced effective gene silencing in MDA-MB-231 cells. These data indicate that αHB-EGF LNP could be internalized in the cells and released siRNA to the cytoplasm successfully. While it remains unclear precisely how the siRNA escaped from the endosomes, it appears that the fusogenic lipid DOPE plays an important role in the system. Even though the LNP-siRNA particles are not likely to interact easily with the endosomal membrane due to their negative charge, the DOPE-rich particles may be destabilizing the membrane with structural changes associated with pH-reduction during endosome maturation[43]. The LNP-siRNA may be able to escape from the endosome due to a conformational change in DOPE. At the same time, Fab'-modified DSPE-PEG might be removed from LNP-siRNA. Control LNP-siPLK1 slightly reduced PLK1 mRNA, which may be due to nonspecific interaction between control Fab' and cell surface proteins. In contrast, αHB-EGF LNP-siCont did not show any gene silencing activity, suggesting that siRNA does not induce sequence-dependent off-target mediated toxicity. As shown in **Figure 2C**, remarkable anti-proliferative effect of MDA-MB-231 cells was observed in HB-EGF LNP-siPLK1-treated group. These data suggest that PLK1 knockdown with αHB-EGF LNP-siPLK1 may be a promising approach for suppression of tumor growth.

[Chapter 2.] Systemic administration of siRNA with anti-HB-EGF antibody-modified lipid nanoparticles for the treatment of triple-negative breast cancer

In this chapter, the αHB-EGF LNP-siRNA was administered to mice grafted with MDA-MB-231 and evaluated its utility as a candidate for TNBC treatment. Biodistribution of radioisotope-labeled lipid or fluorescence-labeled siRNA were analysed to demonstrate that αHB-EGF LNP could deliver siRNA to tumor tissue effectively in MDA-MB-231 carcinoma-bearing model mice. In addition, siRNA against polo-like kinase 1 (siPLK1) formulated in αHB-EGF LNP was intravenously injected to tumor-bearing mice for evaluation of therapeutic effect *in vivo*.

1-[2]-1. Experimental Section

1-[2]-1-1. Materials

[Cholesteryl-1,2-^{3}H(N)]-cholesteryl hexadecyl ether was perchased from PerkinElmer (MA, USA). Alexa750-conjugated siRNA against green fluorescent protein (siGFP) was purchased from Japan Bio Services Co., Ltd. (Saitama, Japan). The nucleotide sequences with a 2-nucleotide overhang (underline) for siGFP were 5'-GGC UAC GUC CAG GAG CGC A<u>CC</u>-3' (passenger) and 5'-UGC GCU CCU GGA CGU AGC C<u>UU</u>-3' (guide). In the *in vivo* experiment, siLuc2, siPLK1 and Alexa750-conjugated siGFP was modified with cholesterol at the 3' end of the passenger strand. For the use of Alexa750-labeled siGFP, Alexa750 was conjugated to siGFP at the 3' end of the guide strand. Suppliers for other materials are as described in Chapter 1.

1-[2]-1-2. Preparation of αHB-EGF LNP-siRNA

Each LNP-siRNA was prepared as described in Chapter 1. To prepare the [^{3}H]-labeled and the fluorescence-labeled LNP-siRNA, [^{3}H]cholesteryl hexadecyl ether and 3,3'-dioctadecyloxacarbocyanine perchlorate (DiO), respectively, were added to the initial lipid solution. For the modification of LNP-siRNA with Fab' fragments of anti-HB-EGF antibody, 1 mL of the LNP-siRNA solution was incubated with 95 μL of 5 mM DSPE-PEG and 5 μL of 5 mM DSPE-PEG-maleimide at 37°C for 2 h, forming PEG-mal-LNP-siRNA. The Fab' fragments and PEG-mal-LNP-siRNA (1/1 as a molar ratio of Fab' and maleimide moiety) were mixed, and the coupling reaction was carried out at 4°C for 16 h to obtain αHB-EGF LNP-siRNA.

1-[2]-1-3. Experimental animals

Four-week-old BALB/c nu/nu female mice were purchased from Japan SLC (Shizuoka, Japan). The animals were cared for according to the Animal Facility Guidelines of the University of Shizuoka. All animal experiments were approved by the Animal and Ethics Committee of the University of Shizuoka on April 1, 2016 (Approval No. 166198). For preparation of tumor-bearing mice, MDA-MB-231 cells (1×10^7 cells/200-μL PBS/mouse) were implanted subcutaneously into the flank of BALB/c nu/nu mice. Each type of LNP-siRNA was administered via a tail vein at selected times after the implantation, as described in each experiment below. Tumor volume was calculated using the following formula: $0.4 \times a \times b^2$ (a, largest diameter; b, smallest diameter).

1-[2]-1-4. Biodistribution of αHB-EGF LNP-siRNA in mice

Four-week-old BALB/c nu/nu female mice were implanted subcutaneously with MDA-MB-231 cells. The mice were intravenously injected with [^{3}H]-labeled PEG

LNP-siRNA, Control LNP-siRNA, or αHB-EGF LNP-siRNA (74 kBq / mouse). At 24 hours after injection, the mice were sacrificed under deep anesthesia with isoflurane (Wako Pure Chemical Industries, Ltd.), and their blood was collected. The collected blood was centrifuged (3,000 rpm, 10 min, 4°C) to obtain plasma. Then, the heart, lungs, liver, spleen, kidneys, and tumor were removed, washed with PBS, and weighed. To lyse them, these excises were treated with Solvable (PerkinElmer). They were then treated with hydrogen peroxide (Wako Pure Chemical Industries, Ltd.) for bleaching. After incubation with Hionic-Fluor (PerkinElmer) overnight at room temperature, the radioactivity in the plasma and in each organ was determined with a liquid scintillation counter (LSC-7400, Hitachi Aloka Medical, Tokyo, Japan). Distribution data were presented as % injected dose per 100 mg tissue. The total amount in the plasma was calculated based on the body weight of the mice, where the plasma volume was assumed to be 4.27% of body weight based on total blood volume.

1-[2]-1-5. Intratumoral distribution of αHB-EGF LNP-siRNA

DiO-labeled Control LNP-siRNA or αHB-EGF LNP-siRNA were injected (10 μg/mouse as siRNA) to MDA-MB-231 carcinoma-bearing mice via a tail vein. Twenty-four hours after injection, the mice were injected with DyLight594®-conjugated *Lycopersicon Esculentum* (Tomato) Lectin (Vector Laboratories, Inc., Burlingame, CA, USA) to stain vessels with blood perfusion. Fifteen minutes later, perfusion fixation of the organs was performed with 1% paraformaldehyde under deep anesthesia with isoflurane, and the tumor was excised. The tumor was then embedded and frozen in Tissue-Tek® O.C.T. Compound (Sakura Finetek Japan, Tokyo, Japan). Frozen tumor sections of 10-μm thickness were prepared with a Microtome HM 505 E Cryostat (Micro-edge Instruments, Tokyo, Japan) and mounted on MAS-coated slides (Matsunami Glass, Osaka, Japan). After being fixed with 1% paraformaldehyde and blocked with 3% bovine serum albumin in PBS, the cell nuclei of the

samples were stained with 4',6-diamidino-2-phenylindole (DAPI, Life Technologies, Carlsbad, CA, USA). Intratumoral distribution of DiO-labeled LNP was observed by confocal laser-scanning microscopy (A1R^{+}, Nikon, Tokyo, Japan).

1-[2]-1-6. siRNA distribution in tumor-bearing mice

MDA-MB-231 carcinoma-bearing BALB/c *nu/nu* mice were prepared and injected with Alexa750-labeled naked siRNA, Alexa750-labeled siRNA formulated in Control LNP, or αHB-EGF LNP (10 μg / mouse as siRNA) intravenously on the day when the tumor had reached a volume of approximately 300 mm^3. Biodistribution of Alexa750-labeled siRNA was then measured with an *in vivo* imaging system (Xenogen IVIS Lumina System) coupled to Living Image software for data acquisition (Xenogen Corp., Alameda, CA, USA) with 30 seconds exposure for each imaging point. Twenty-four hours after the injection, perfusion fixation of the organs was performed with 1% paraformaldehyde under deep anesthesia with isoflurane. The organs and tumor were excised, and their fluorescence intensities were determined by IVIS.

1-[2]-1-7. Protein knockdown effect of αHB-EGF LNP-siPLK1 in tumor-bearing mice

MDA-MB-231 carcinoma-bearing mice were injected with αHB-EGF LNP-siCont, Control LNP-siPLK1, or αHB-EGF LNP-siPLK1 intravenously (10 μg/mouse as siRNA) on the day when the tumor had reached a volume of approximately 250 mm^3. Five days after treatment, the tumor was collected and homogenized in Tissue-Protein Extraction Reagent (Thermo Fisher Scientific Inc., Kanagawa, Japan) containing protease inhibitors using a Shakeman 2 vortex homogenizer (Biomedical Science, Tokyo, Japan) for 2 cycles of homogenization: 40 seconds of shaking, then 20 seconds of cooling on ice. The homogenate was centrifuged 3 times (10,000 x*g*, 10 min, 4°C) in order to obtain the tumor protein

extraction. The protein concentration of the extraction was determined by BCA assay. Thirty micrograms of the protein was applied to 10% SDS-PAGE. Expression of PLK1 and β-actin was determined by Western blotting. Immunoblotting was performed with a primary antibody against PLK1 (1:2,000) or β-actin (1:10,000) overnight at 4°C, and then with an HRP-conjugated secondary antibody (1:10,000) for 1 h at room temperature.

1-[2]-1-8. Therapeutic experiment

MDA-MB-231 carcinoma-bearing mice were injected with samples (αHB-EGF LNP-siCont, Control LNP-siPLK1, or αHB-EGF LNP-siPLK1) on the days 17, 24, 31 and 38 after the implantation (10 μg/mouse as siRNA dose per day). The tumor size and body weight of each mouse were monitored daily from one day before sample injection. As an experimental control, PBS was injected instead of the LNP-siRNA samples.

1-[2]-1-9. Statistical analysis

Differences within a group were evaluated by analysis of variance (ANOVA) with the Tukey *post-hoc* test.

1-[2]-2. Results

1-[2]-2-1. Biodistribution of αHB-EGF LNP in tumor-bearing mice

αHB-EGF LNP was examined whether it can be applied to systemic delivery of siRNA. Experimental procedures are shown in **Figure 3A**. [^{3}H]-labeled αHB-EGF LNP-siRNA showed significantly higher retention in plasma than PEG LNP-siRNA without antibodies at 24 h after administration. Control LNP-siRNA also showed slightly higher retention in plasma than PEG LNP-siRNA (**Figure 3B**). Antibody-conjugation did not result in an undesirable effect on the circulation of LNP-siRNA in the blood. In addition, there were no significant differences in tumor accumulation between the three LNPs (**Figure 3B, enlarged view**). αHB-EGF LNP-siRNA accumulated in the tumor at a slightly higher level than the other LNPs. About 0.3% of αHB-EGF LNP-siRNA accumulated per 100 mg of tumor tissue.

In addition, to observe the intra-tumor distribution of αHB-EGF LNP-siRNA, DiO-labeled αHB-EGF LNP-siRNA or Control LNP-siRNA were injected into MDA-MB-231 carcinoma-bearing mice. After sacrifice, frozen slices of the tumors examined by confocal laser-scanning microscope showed that DiO-labeled αHB-EGF LNP-siRNA accumulated more densely around blood vessels compared with DiO-labeled Control LNP-siRNA (**Figure 3C**). Additionally, in the experimental group, αHB-EGF LNP-siRNA was densely distributed, even over tumor tissue at a considerable distance from blood vessels (shown with arrows), while in the control group there was no obvious accumulation deep in the tumor. There were also no significant differences in blood vessel formation.

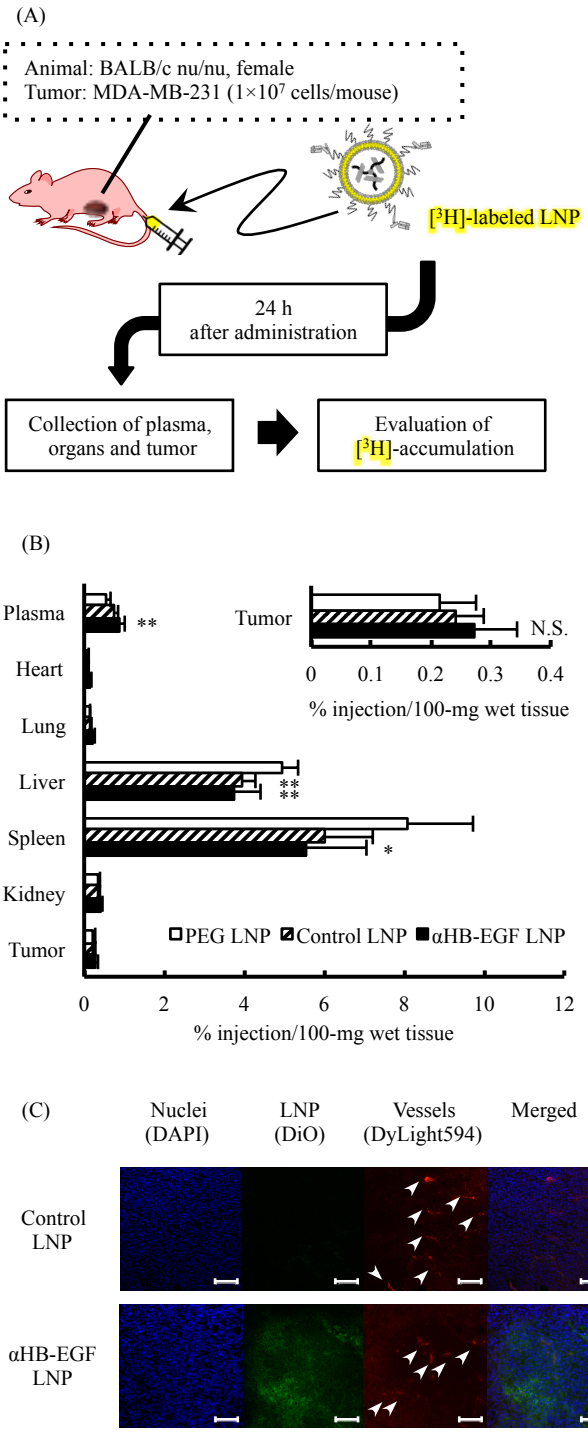

Figure 3. Delivery of siRNA to tumors *in vivo* using αHB-EGF LNP. (A) Schematic image of the experiments. MDA-MB-231 cells were subcutaneously injected into BALB/c *nu/nu* mice. [^{3}H]-labeled PEG LNP-siRNA, Control LNP-siRNA or αHB-EGF LNP-siRNA was intravenously injected into tumor-bearing mice (74 kBq/mouse) when the tumor volume had reached around 300 mm^3. (B) Biodistribution of LNP-siRNA at 24 h after injection in MDA-MB-231-bearing mice. The data are shown as mean ± S.D. (n=6). Asterisks indicate significant differences (*P<0.05, **P<0.01 *vs.* PEG LNP-siRNA). (C) Intratumoral distribution of αHB-EGF LNP-siRNA after intravenous injection. MDA-MB-231-bearing mice were administrated with DiO-labeled Control LNP-siRNA, or DiO-labeled αHB-EGF LNP-siRNA (green). After 24 h, vessels were perfused with PBS and stained by intravenous injection of DyLight594-conjugated tomato lectin (red). The nuclei were counterstained with DAPI (blue). Accumulation of DiO-labeled LNP in the tumor was observed using a confocal laser-scanning microscope. Arrows show the vessels with blood circulation. The scale bars indicate 100 μm.

1-[2]-2-2. Biodistribution of siRNA formulated in αHB-EGF LNP

In order to directly assess siRNA distribution *in vivo*, non-invasive imaging using Alexa750-labeled siRNA was carried out (**Figure 4A**). After injection, Alexa750-naked siRNA spread quickly throughout the whole body, and most of it was eliminated by 3 h (**Figure 4B**). Control LNP-siRNA and αHB-EGF LNP-siRNA showed almost the same distribution in mice. Although images taken 24 h after injection showed similar levels of siRNA accumulation in the tumors, *ex vivo* imaging showed that the siRNA formulated in αHB-EGF LNP-siRNA accumulated in the tumor more effectively than that in the other types (**Figure 4C**).

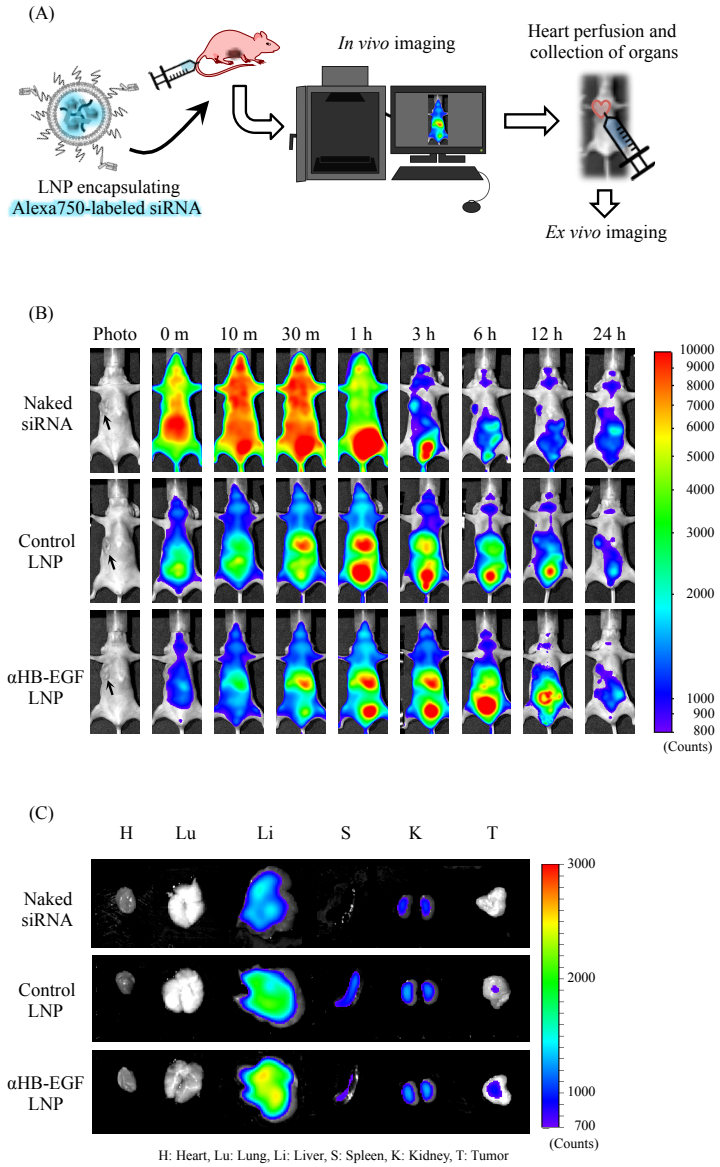

Figure 4. In vivo and ex vivo imaging of siRNA administered to tumor-bearing mice. (A) Schematic illustration of the experimental procedure. (B) siRNA distribution in MDA-MB-231 carcinoma-bearing mice. The mice were injected with Alexa750-labeled naked siRNA, or Alexa750-labeled siRNA in Control LNP or αHB-EGF LNP via the tail vein. Biodistribution of Alexa750-siRNA was measured using the IVIS at indicated time. Arrows indicate tumors. (C) *Ex vivo* images of siRNA distribution in each organ. These mice were heart-perfused with PBS at 24 h after the injection. Fluorescence intensity of Alexa750-siRNA in each organ and tumor was determined using the IVIS.

1-[2]-2-3. Protein knockdown effect of αHB-EGF LNP-siPLK1 *in vivo*

The potential of αHB-EGF LNP-siPLK1 as an RNAi-based drug was evaluated *in vivo*. αHB-EGF LNP-siCont, Control LNP-siPLK1, or αHB-EGF LNP-siPLK1 were intravenously administered to MDA-MB-231 tumor-bearing mice at a dose of 0.5 mg/kg siRNA. Evaluation of PLK1 expression by Western blotting clearly showed the suppression of PLK1 protein expression in the αHB-EGF LNP-siPLK1-treated tumor (**Figure 5**). Treatment with αHB-EGF LNP-siCont or Control LNP-siPLK1 induced no silencing effects in PLK1 protein in the implanted tumors.

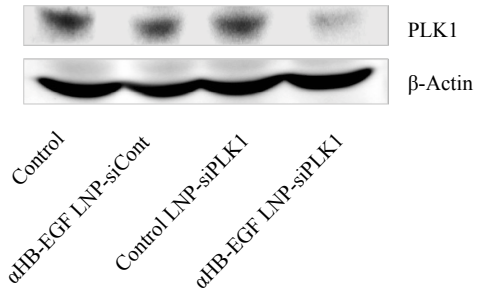

Figure 5. Knockdown effect of αHB-EGF LNP-siPLK1 *in vivo*. MDA-MB-231 carcinoma-bearing mice were injected with αHB-EGF LNP-siCont, Control LNP-siPLK1, or αHB-EGF LNP-siPLK1 via the tail vein. The tumor was collected and homogenized at 5 days after treatment. PLK1-protein expression was determined by Western blotting.

1-[2]-2-4. Therapeutic effect of αHB-EGF LNP-siPLK1

Finally, the therapeutic effect of αHB-EGF LNP-siPLK1 was evaluated in tumor-bearing mice. Mice treated with αHB-EGF LNP-siPLK1 showed significantly stronger suppression of tumor growth than non-treated mice, and a tendency towards tumor growth suppression was greater in the αHB-EGF LNP-siPLK1-treated group than in the αHB-EGF LNP-siCont-treated and Control LNP-siPLK1-treated groups (**Figure 6A**). The body weight of the mice treated with αHB-EGF LNP-siCont, Control LNP-siPLK1, and αHB-EGF LNP-siPLK1 was temporarily slightly reduced in the days after injection, but recovered within 1 week (**Figure 6B**).

(A)

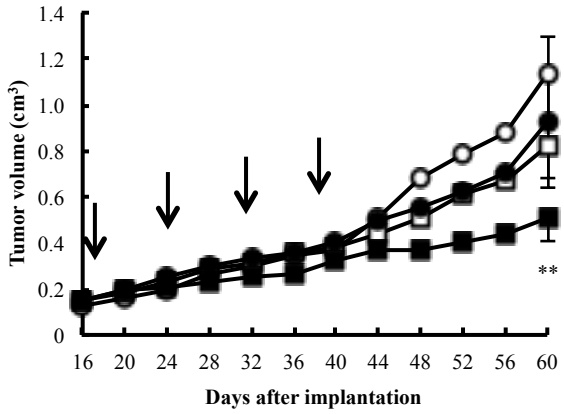

(B)

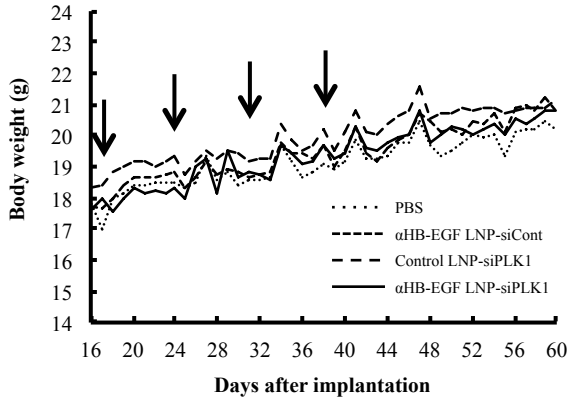

Figure 6. Anticancer effect of αHB-EGF LNP-siPLK1 *in vivo.* (A) MDA-MB-231 carcinoma -bearing mice were injected 4 times with PBS (○), αHB-EGF LNP-siCont (□), Control LNP-siPLK1 (●), or αHB-EGF LNP-siPLK1 (■) once a week. The tumor size of each mouse was monitored from day 16. Arrows indicate the days of treatment. Asterisk indicates significant difference (*P<0.05 *vs.* PBS). (B) Body weight of the treated mice was also monitored.

1-[2]-3. Discussion

In this study, αHB-EGF LNP loaded with siRNA against polo-like kinase 1 (siPLK1) was developed for the treatment of MDA-MB-231 breast cancer cells, one of TNBC cells expressing HB-EGF on their cell surface. αHB-EGF LNP-siPLK1 were administered to MDA-MB-231 carcinoma-bearing mice and evaluated its utility as a candidate for TNBC treatment. αHB-EGF LNP was examined whether it can be applied to systemic delivery using MDA-MB-231 carcinoma-bearing mice. **Figure 3B** indicates that antibody-conjugation did not reduce the circulation of Control LNP-siRNA or αHB-EGF LNP-siRNA in the blood. Unmodified LNP-siRNA showed blood retentivity of 0.1% at 24 h after injection (data not shown). PEG LNP-siRNA, Control LNP-siRNA, and αHB-EGF LNP-siRNA showed from 6- to 9-times higher retention than unmodified LNP-siRNA at this time point. Tumor accumulation was almost the same in the three groups. These LNP-siRNA would be able to accumulate in the tumor via the EPR effect. Further experiments are required to clarify the reason why αHB-EGF LNP-siRNA showed longer blood circulation and lower accumulation in the liver and spleen than PEG LNP-siRNA. As shown in **Figure 3C**, αHB-EGF LNP-siRNA dispersed more deeply into the tumor than Control LNP-siRNA, suggesting that αHB-EGF LNP binds HB-EGF on the surface of MDA-MB-231, stays under elevated interstitial pressure within tumors, and delivers siRNA more densely into tumor cells than the other formulations. As **Figure 1** showed that αHB-EGF LNP-siRNA significantly binds to and is taken up into MDA-MB-231 cells compared with Control LNP *in vitro*, it is likely that αHB-EGF LNP-siRNA was taken up into MDA-MB-231 cells more effectively than Control LNP-siRNA after accumulation in the tumor. These results demonstrated that anti-HB-EGF-antibody may be useful for the delivery of LNP into tumor tissue *in vivo*.

Figure 4B indicates that siRNA formulated in αHB-EGF LNP or Control LNP

exhibited a longer systemic circulation than naked siRNA, although a part of siRNA might be released from LNP in the blood, accumulated in the bladder, and excreted into the urine. *Ex vivo* images in **Figure 4C** suggest that the naked siRNA and Control LNP-siRNA may have been swept away by PBS because these nanoparticles have no specific ligands. In contrast, αHB-EGF LNP-siRNA bound cooperatively to HB-EGF on the surface of MDA-MB-231 cells. This strong interaction between αHB-EGF LNP-siRNA and MDA-MB-231 cells appears to have resulted in effective retention in tumor tissue compared with the other groups. While TNBC does not possess general address molecules such as estrogen receptor (ER), progesterone receptor (PR), or human epidermal growth factor receptor 2 (HER2), these results suggest that HB-EGF can be an effective address molecule for targeted TNBC therapy.

Finally, the gene silencing ability of αHB-EGF LNP *in vivo* was determined. **Figure 5** showed that the expression of PLK1 protein was remarkably reduced only in αHB-EGF LNP-siPLK1-treated tumor. This indicates that αHB-EGF LNP-siPLK1 induced an RNA interference effect in a ligand-specific and a sequence-dependent manner. An experiment to confirm whether PLK1 expression changes in the liver was conducted by Western blotting, but the signal of PLK1 protein expression was not detected. This is probably because the expression level of PLK1 is not enough to detect in normal tissues. It was reported that expression of PLK1 was not observed in normal liver while high PLK1 expression was detected in cancerous one[44,45]. In addition, it has also been reported that the expression level of HB-EGF mRNA and protein was very low in normal liver tissue[46]. Our group previously revealed that anti-HB-EGF Fab'-modified liposomes bound to and were taken up into HB-EGF-expressing Vero (Vero-H) cells, but not into native Vero cells[35]. These results indicate that the anti-HB-EGF antibody may enable tumor-targeted drug delivery without carrier-dependent toxicity. αHB-EGF LNP-siPLK was also confirmed whether it could effectively treat TNBC *in vivo*. As shown in **Figure 6**, αHB-EGF LNP-siPLK1 significantly

suppressed tumor growth without significant body weight loss. In the αHB-EGF LNP-siCont-treated group, tumor volume was slightly decreased. Neutralizing activity of HB-EGF antibody on the surface of LNP-siCont might affect and suppress tumor growth after administration of αHB-EGF LNP-siCont. Control-LNP-siPLK1 also slightly suppressed tumor growth, suggesting that certain amount of Control LNP-siPLK1 might be taken up into tumor cells in a nonspecific manner. Another possibility is that natural killer cells were activated and attacked cancer cells after treating with each LNP-siRNA[47]. Although further investigations for appropriate formulation design may be required, gene silencing with αHB-EGF LNP-siPLK1 appears to be an attractive approach for the treatment of TNBC.

Importantly, αHB-EGF LNP-siRNA may show even more effective tumor suppression activity in clinical TNBC patients than in animal models. Previous studies have found tumor proliferation and angiogenesis in tumor xenograft model animals to be somewhat different from that in homograft and spontaneous models[48,49]. In the present study, human HB-EGF was expressed on the surface of MDA-MB-231 human TNBC cells, but was not expressed on cells originating from mice. It is known that the anti-HB-EGF antibody clone 3E9 is able to specifically bind to human HB-EGF, which explains why αHB-EGF LNP-siRNA targeted MDA-MB-231, but did not target other tumor-associated cells in our experiment. HB-EGF is also known to be expressed on the surface of human angiogenic vessels[25] and stromal cells[50]. Taken together, it is suggested that αHB-EGF LNP is a unique drug delivery system that can target not only cancer cells themself but also tumor-associated cells that construct tumor microenvironment of TNBC.

Part 1. - Conclusion

This study has demonstrated both *in vitro* and *in vivo* that anti-HB-EGF antibody-modified lipid nanoparticles encapsulating siRNA (αHB-EGF LNP-siRNA) are likely to be an effective treatment for triple-negative breast cancer via an RNAi-mediated gene-silencing effect. αHB-EGF LNP-siPLK1 was taken up into MDA-MB-231 triple-negative breast cancer cells, and induced a strong RNA interference effect *in vitro*. The ability of these nanoparticles to systemically deliver siRNA was confirmed with *in vivo* experiments on long-term blood circulation and tumor tissue accumulation using radioisotope-imaging of LNP and fluorescence-imaging of siRNA. In addition, treatment of MDA-MB-231 carcinoma-bearing mice with αHB-EGF LNP-siPLK1 clearly suppressed PLK1 protein expression and tumor growth. These findings suggest that gene silencing with αHB-EGF LNP-siPLK1 is a promising approach to the treatment of triple-negative breast cancer.

Part 2. Rigorous control of vesicle-forming lipid pK_a by fluorine substitution, and evaluation of its effect on siRNA delivery

Part 2. - Introduction

In order to induce target mRNA degradation by siRNA, siRNA has to hurdle the multiple steps including as follows: 1) being taken up into cell, 2) escaping from the endosome, and 3) being released to the cytoplasm[51]. Unfortunately, the physicochemical properties of siRNA such as high molecular weight, hydrophilicity and high negative charge density make it difficult to break these steps by themselves. Therefore, delivery technology is indispensable for practical application of siRNA, and various materials such as liposomes[52], lipid nanoparticles[53], polymer nanoparticles[54], dendrimers[55], and nanogels[56] have been studied widely as siRNA carrier.

Polyethylenimine has been widely used as a positively charged group for the siRNA-holding in the carrier. Although transfecting siRNA with polyethylenimine-containing nanocarriers bring significant gene-silencing effect by increasing siRNA uptake into the cell and endosome escape[57], its strong cytotoxicity has been a critical problem[58]. Therefore, a number of studies have been carried out to reduce the toxicity and enhance the knockdown effect by the improvement of polycation structure. For example, Kataoka's group has prepared a series of the *N*-substituted polyaspartamides possessing repeating aminoethylene units[59]; Hope's group synthesized 56 amino lipids that include primaty, secondly and tertiary amine residue[60]; Langer and Anderson's group prepared a large library of lipidoid containing a secondary or a tertiary amine residue[61]; Harashima's group synthesized dimethylamino lipids containing different numbers of methylene units[62]; Siegwart's group synthesized 139 lipocationic polyesters containing dialkyl amine or heterocyclic amine polymer[63]. These

reports indicate that amine pK_a (pK_a 6.2-6.5) is important for the efficient gene-silencing and reduction of the toxicity. However, precise regulation of the amine pK_a without significant change of chemical structure is considered to be extremely difficult, since the adjustment of the amine pK_a usually requires conjugation of bulky groups such as alkyl chain, benzene, cycloalkane or bicyclo-compound to the amine group[60,61]. Such modification changes steric bulk of the molecules along with the pK_a. It is known that steric bulk significantly affects on the gene-silencing effect[61]. Therefore, rigorous control of amine pK_a without drastic structural change, and investigation of the amine pK_a influence on gene-silencing effect is still of great challenge and important for the designing of siRNA carrier.

In the present study, the fluorine atom was focused on for the rigorous control of amine pK_a. As the fluorine atom is a strong electron-withdrawing substituent and has a similar atomic size with hydrogen[64], the pK_as of conjugate acids derived from neighboring nitrogen atoms decrease accordingly with the number of fluorine atoms without significant change of chemical structure and steric bulk[65]. Ethylenediamine (EDA) was used as a model of amine group. In addition, diethylenetriamine (DETA) was used to examine the effect of the number of amine on the gene-silencing.

2-1. Experimental Section

2-1-1. Materials

Dicetylphosphate-ethylendiamine-CH_2R conjugate and dicetylphosphate-diethylentriamine-CH_2R conjugate (R indicates: $-CH_3$, $-CH_2F$, $-CHF_2$, $-CF_3$) were synthesized and kindly provided by Mr. Naoki Morita and Prof. Yoshitaka Hamashima at Department of Synthetic Organic Chemistry, University of Shizuoka. Distearoylphosphatidylethanolamine-polyethyleneglycol 2000 (DSPE-PEG2000), dioleoylphosphatidylethanolamine (DOPE), dipalmitoylphosphatidylcholine (DPPC), and cholesterol were kindly provided by Nippon Fine Chemical Co. (Hyogo, Japan). Chloroform, *t*-butanol, sodium dihydrogen phosphate, disodium phosphate, sodium hydroxide (NaOH), hydrochloric acid (HCl), sodium chloride (NaCl), sucrose, GelRed and D-MEM/Ham's F-12 were purchased from Wako Pure Chemical Industries, Ltd. (Osaka, Japan). Liquid nitrogen was obtained from Marukyo Sanso Co., Ltd. (Shizuoka, Japan). UltraPure™ DNase/RNase-Free Distilled Water (RNase-free water), Pierce™ BCA Protein Assay Reagent Kit was purchased from Thermo Fisher Scientific Inc. (Kanagawa, Japan). siRNA against green fluorescent protein (siGFP) and against luciferase 2 (siLuc2) were purchased from Hokkaido System Science Co. (Hokkaido, Japan). The nucleotide sequences with a 2-nucleotide overhang (underline) for siGFP were 5'-GGC UAC GUC CAG GAG CGC A<u>CC</u>-3' (passenger) and 5'-UGC GCU CCU GGA CGU AGC C<u>UU</u>-3' (guide), and for siLuc2 were 5'-GCU AUG GGC UGA AUA CAA A<u>TT</u>-3' (passenger) and 5'-UUU GUA UUC AGC CCA UAG C<u>TT</u>-3' (guide). For the use of fluorescein isothiocyanate (FITC)-labeled siRNA, FITC was conjugated to siLuc2 at the 3' end of the guide strand. Cell-penetrating peptide-conjugated DOPE (CPP-DOPE) was synthesized as previously[66]. The amino acid sequence of CPP was RRRRRRGGRRRRG. HT1080 human fibrosarcoma

cells were perchased from ATCC (Manassas, VA). HT1080 cells constitutively expressing enhanced green fluorescent protein (HT1080-EGFP cells) had been previously established[67]. Fetal bovine serum (FBS) was obtained from AusGeneX Pty. Ltd. (Brisbane, Australia). Penicillin G and streptomycin were obtained from MP Biomedicals (Santa Ana, CA, U.S.A.). Heparin was purchased from Mochida Pharmaceutical Co., Ltd. (Tokyo, Japan). *n*-Octyl-*β*-D-glucoside and Cell Counting Kit-8 were perchased from Dojindo Laboratories Co., Ltd. (Kumamoto, Japan). 6-(*p*-Toluidino)-2-naphthalenesul-fonic acid (TNS), phenylmethylsulfonyl fluoride (PMSF), leupeptin, aprotinin, pepstatin A and Triton X-100 were purchased from Merck KGaA (Darmstadt, Germany). Bovine blood (Lot. 025-0703) was pharchased from Nippon Bio-Test Labolatories, Inc. (Saitama, Japan).

2-1-2. Titration of polyamine-lipid

DCP-polyamine-CH_2R and DSPE-PEG2000 (1/0.1 as a molar ratio) were dissolved in *t*-butanol and lyophilized. Liposomes were produced by hydration of the lipid mixture with RNase-free water. PEG-DCP-EDA-CH_2R or PEG-DCP-DETA-CH_2R were diluted (final lipid conc.: 2 mM) with 5 mL of ultra pure water containing 150 mM NaCl, and basified with 0.1 M NaOH. Five μL of 0.1 M HCl was added to the vial by use of micropipette while stering the solution. pH change was monitored by use of pH meter HM-31P (DKK-TOA, Tokyo, Japan). After stabilized the pH, additional HCl was droped.

2-1-3. Liposome formulations

DOPE, cholesterol, DPPC and DCP-EDA-CH_2CF_3 (1/1/0/1, 1/1/0.25/0.75, or 1/1/0.5/0.5 as molar ratio) were dissolved in *t*-butanol and freeze-dried. Liposomes were produced by hydration of the lipid mixture with RNase-free water. After 3 cycles of freeze-thaw, liposomes were sized by extrusion. The particle size and ζ-potential of the

complexes diluted with RNase-free water was measured by use of Zetasizer Nano ZS (Malvern, Worcs, UK).

2-1-4. TNS assay

DOPE, cholesterol, DPPC and polyamine lipid (1/1/0.5/0.5 as a molar ratio) were dissolved in *t*-butanol and freeze-dried. Liposomes were produced by hydration of the lipid mixture with RNase-free water. Ten μL of 1 mM LVs were diluted in 480 μL of assay buffer containing 20 mM sodium phosphate, 25 mM citrate, 20 mM ammonium acetate, 150 mM NaCl (pH 2.0-12.0), and incubated for 20 min at room temperature. Then, 10 μL of 0.3 mM 6-(*p*-toluidino)-2-naphthalenesul-fonic acid (TNS) was mixed with the LVs solutions. The fluorescence intensity of TNS was determined with a Tecan Infinite M200 microplate reader (Salzburg, Austria) operated according to the manufacturer's instructions (ex. 322 nm, em. 431 nm).

2-1-5. Preparation of siRNA-encapsulated lipid vesicles

siRNA-encapsulated lipid vesicles (siRNA-LVs) was prepared by freeze-thawing of siRNA and liposome complex as described previoiusly[68]. Liposomes and siRNA were mixed (nitrogen/phosphorus ratio; N/P ratio = 20) and incubated for 20 min at room temperature in RNase-free water or 1 mM citric acid/RNase-free water to form siRNA/liposome complexes. To prepare freeze-thawed LVs, the complex was frozen in liquid nitrogen and thawed in a water bath at 45°C with vortexing. siRNA-LVs were decorated with CPP-DOPE conjugate (6 mol% to total lipids) by incubating them at 50°C for 30 min (EDA-LVs-CPP, DETA-LVs-CPP) on demand. The ζ-potential of the complexes diluted with 10 mM phosphate buffer (pH = 5.5 or 7.4) was measured by use of Zetasizer Nano ZS (Malvern).

2-1-6. Electrophoretic assay

siRNA that was not or loosely attached to liposome was checked by performing 15% polyacrylamide gel electrophoresis, where the siRNA in stable complexes did not enter the gel. The gel was stained for 30 min in GelRed, and siRNA was detected by using a LAS-3000 mini system (Fuji Film, Tokyo, Japan).

2-1-7. Cell culture

HT1080 cells and HT1080-EGFP cells were cultured respectively in D-MEM/Ham's F-12 supplemented with 10% FBS, 100-units/mL penicillin G, and 100-μg/mL streptomycin in a CO_2 incubator.

2-1-8. siRNA transfection

Cells were seeded onto a culture plate and pre-cultured overnight. The medium was changed to a fresh one containing FBS but not antibiotics (adjusted pH 7.4) before transfection. EDA-LVs-CPP or DETA-LVs-CPP was added to the culture medium at a final concentration of 10 nM as siRNA (5 pmol/500 μL), and the cells were then incubated for 24 h at 37°C in a 5% CO_2 incubator. After a medium change, the cells were incubated for the desired time as described for each experimental procedure.

2-1-9. Association of siRNA-LVs-CPP with cells

HT1080 cells were seeded onto 24-well plates (BD Bioscience, San Jose, CA) at the density of 1.5×10^4 cells/well. FITC-labeled siRNA formulated in freeze-thawed LVs were added to the cells (5 pmol/500 μL; 10 nM as siRNA). Twenty-four hours after the transfection, the cells were washed with PBS containing 30 units/mL heparin and lysed with 1 w/v% *n*-octyl-*β*-D-glucoside containing the following protease inhibitors: 1 mM PMSF, 2 μg/mL

leupeptin, 2 μg/mL aprotinin, and 2 μg/mL pepstatin A. The fluorescence intensity of FITC was determined with a Tecan Infinite M200 microplate reader (Salzburg, Austria) operated according to the manufacturer's instructions (ex. 495 nm, em. 535 nm). Total protein contents were measured with a Pierce™ BCA Protein Assay Reagent Kit according to the manufacturer's instructions.

2-1-10. Gene-silencing effect and cytotoxicity of siRNA-LVs-CPP

HT1080-EGFP cells (1.5×10^4 cells/well) were seeded onto 24-well plates (BD Bioscience) and transfected with siGFP formulated in each LVs-CPP for 24 h at a final siRNA concentration of 10 nM (5 pmol/500 μL). After these complexes had been removed, the cells were cultured for an additional 48 h. Cell viability was determined by WST-8 assay; the media was changed to WST-8 assay reagent (Cell Counting Kit-8 : medium = 7.5 μL : 292.5 μL), and then the cells were incubated for 1 h at 37°C. To determine cell viability, absorbance of supernatant at 450 nm was measured using Tecan Infinite M200 microplate reader. Then, the cells were washed with PBS and lysed with 1 w/v% *n*-octyl-*β*-D-glucoside containing the protease inhibitors. The fluorescence intensity of EGFP was determined with a Tecan Infinite M200 microplate reader (ex. 485 nm, em. 535 nm). Total protein contents were measured with a Pierce™ BCA Protein Assay Reagent Kit. RNA interference efficiency was determined as follows: Knockdown (%) / siRNA uptake (pmol/well).

2-1-11. Hemolysis assay

For preparation of erythrocyte, 500 μL of blood was washed by gently vortexing with 1 mL of PBS, and was centrifuged at 10,000 ×*g* for 10 min at 4°C. After repeating the wash with PBS five times, the pellet was resuspended with 0.3 M scrose in ultra-pure water. siRNA-LVs-CPP diluted with 10 mM phosphate buffer (pH 7.4 or 5.5) containing 0.3 M

scrose were mixed with 10 μL of the erythrocyte, and incubated at 37°C for 1 h in a shaking container (100 μM as amine moiety). After centrifugation (10,000 ×*g*, 10 min, 25°C), the liberated hemoglobin was determined by colorimetric analysis of the supernatant at 405 nm with a Tecan Infinite M200 microplate reader. The value for 100% hemolysis was set from the erythrocytes treated with 0.1% Triton X-100. The results are presented as the mean ± S.D.

2-1-12. Isothermal titration calorimetric analysis

Isothermal titration calorimetry was performed with MicroCal PEAQ-ITC (Malvern). Temperature was fixed at 25°C. Themally equilibrated cell was filled with 280 μL of 300 nM siRNA solution in 1 mM phosphate buffer (pH 7.4 or 5.5). EDA-liposome or DETA-liposome was titrated into the cell according to the manufactual program. Data analysis was performed by use of the software MicroCal PEAQ-ITC Analysis (Malvern).

2-1-13. Confocal laser-scanning microscopic observation of siRNA

HT1080 cells were seeded onto glass bottom 24-well plate (AGC Techno Glass Co., Ltd., Shizuoka, Japan) at a density of 1.5×10^4 cells/well and precultured overnight. FITC-labeled siRNA-encapsulating EDA-LVs-CPP or DETA-LVs-CPP were added to the cells (FITC-siRNA concentration was 10 nM; 5 pmol/500 μL). Distribution of FITC-labeled siRNA in the HT1080 cells was observed using an $A1R^+$ confocal laser-scanning microscope (Nikon, Tokyo, Japan). Individual cells within a single field of view were imaged every 5 min for 24 h..

2-1-14. Statistical analysis

Differences within a group were evaluated by analysis of variance (ANOVA) with the Tukey *post-hoc* test.

2-2. Results

2-2-1. Characteristics of fluorine-conjugated polyamine lipid

Chemical structures of the synthesized polyamine lipids, DCP-EDA-CH_2R; DCP-DETA-CH_2R (R indicates: -CH_3, -CH_2F, -CHF_2 or -CF_3), were shown in **Figure 7**. To determine the pK_a of synthesized polyamine lipids, acid-base titration was performed using 0.1 M HCl. While the titration curves of EDA-lipids showed a single equivalence point and DETA-lipids showed a two-phase equivalence curve (**Figure 8**). The pK_a of EDA-lipids was gently shifted to lower value by the increasing fluorine atom number from 8.2 (EDA-CH_2CH_3) to 5.3 (EDA-CH_2CH_2F), 4.4 (EDA-CH_2CHF_2), and < 3.3 (EDA-CH_2CF_3), respectively (**Table 2**). Both pK_{a1} and pK_{a2} of DETA-lipids were also shifted to lower value from 9.2 and 5.4 (DETA-CH_2CH_3) to 8.0 and 4.9 (DETA-CH_2CH_2F), 7.5 and 3.9 (DETA-CH_2CHF_2), and 7.1 and < 3.0 (DETA-CH_2CF_3), respectively. pK_a of EDA-CH_2CF_3 and pK_{a2} of DETA-CH_2CF_3 could not be determined.

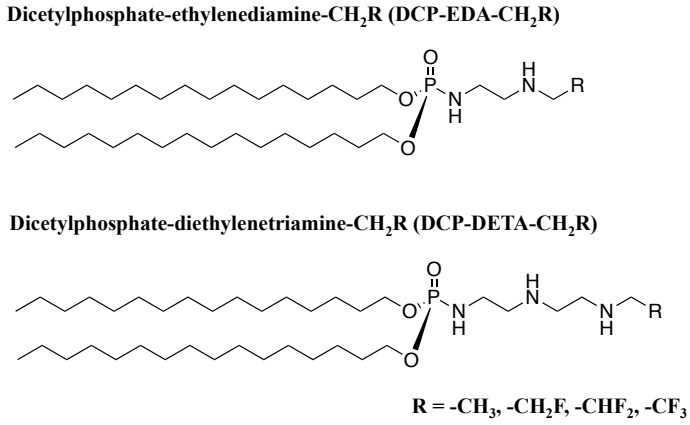

Figure 7. Polyamine lipids with fluormethyl moiety conjugation

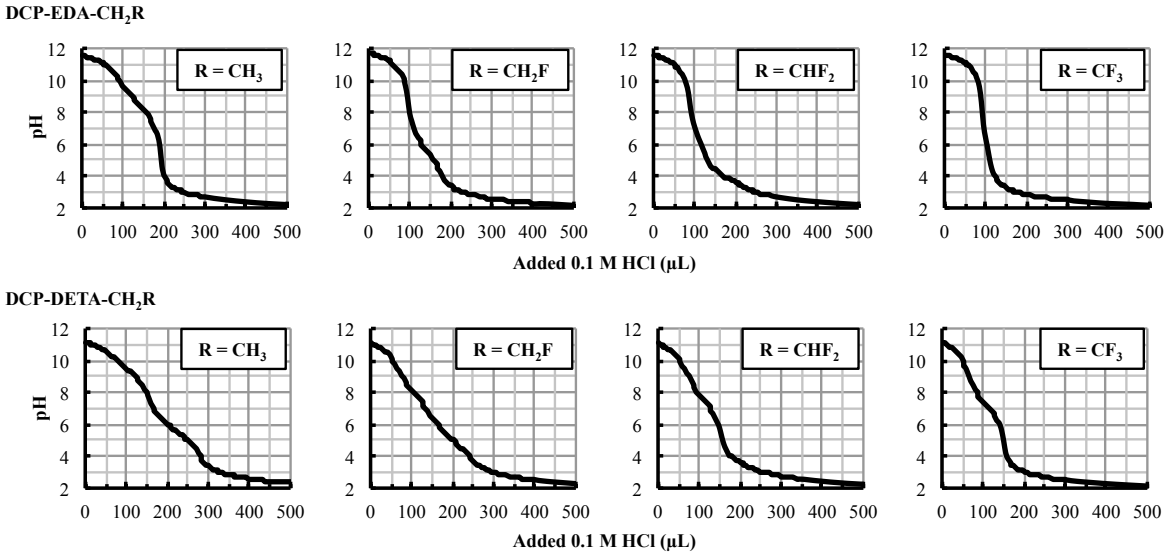

Figure 8. pK_a determination of polyamine lipids
Liposomes (DCP-EDA-CH_2R or DCP-DETA-CH_2R / DSPE-PEG2000 = 10 / 1 as a molar ratio) were diluted with 5 mL of ultra pure water containing 150 mM NaCl, and basified with NaOH. Titration was performed with 0.1 M HCl.

Table 2. pK_a value of cationic lipid

DCP-EDA-CH_2R			DCP-DETA-CH_2R		
R	pK_{a1}	pK_{a2}	R	pK_{a1}	pK_{a2}
CH_3	8.2	-	CH_3	9.2	5.4
CH_2F	5.3	-	CH_2F	8.0	4.9
CHF_2	4.4	-	CHF_2	7.5	3.9
CF_3	< 3.3	-	CF_3	7.1	< 3.0

2-2-2. Preparation of polyamine lipid-containing liposome

Lipid composition for experimental use was determined as DOPE / cholesterol / DPPC / Polyamine lipid = 1/1/0.5/0.5 as a molar ratio because liposome containing DCP-EDA-CH_2CF_3 could not be prepared with other compositions; DOPE / cholesterol / Polyamine lipid = 1/1/1 or DOPE / cholesterol / DPPC / Polyamine lipid = 1/1/0.25/0.75 (**Table 3**).

Table 3. Preparation of EDA-CH_2CF_3-containing liposome

	Lipid composition (molar ratio)				Properties of liposome	
	DOPE	Cholesterol	DPPC	DCP-EDA-CH_2CF_3	Size (d.nm)	PdI
(a)	1	1	0	1	N.A.	N.A.
(b)	1	1	0.25	0.75	N.A.	N.A.
(c)	1	1	0.5	0.5	125.9	0.151

2-2-3. Determination of the liposomal surface charge by TNS assay

Each polyamine liposome composed of DOPE, cholesterol, DPPC, and polyamine lipid (1/1/0.5/0.5 as a molar ratio) was prepared. Charged percentage of the liposomes within pH 2–12 was measured using TNS. Although the curve of EDA-liposomes shifted to low pH side by increasing the number of fluorine atom, that of DETA-liposomes did not show considerable change (**Figure 9**).

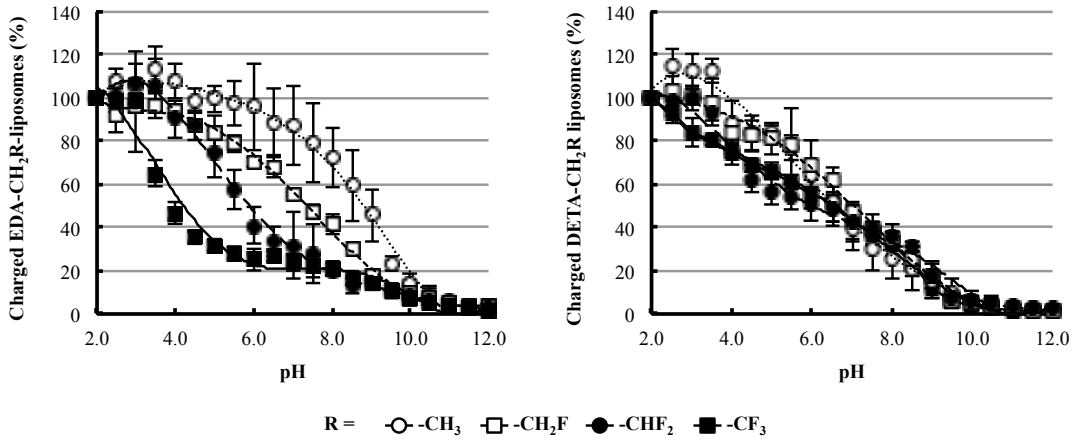

Figure 9. Surface charge of liposomes determined by TNS assay
TNS was mixed with lipid vesicles in a series of buffers with pH ranging between 2 and 12. Fluorescence intensity was normalized by the TNS fluorescence value at pH 2.0.

2-2-4. Preparation of siRNA-encapsulated lipid vesicles by freeze-thawing

In order to prepare siRNA-encapsulated lipid vesicles (siRNA-LVs), siRNA/liposome complex was freeze-thawed for 3 times (**Scheme 2**). Entrapment of siRNA into LVs was examined by electrophoresis (**Figure 10**). When the siRNA/liposome complex was prepared in water, the siRNA band was clearly observed in the siRNA/EDA-CH_2CF_3-liposome group with or without freeze-thawing. In contrast, the siRNA band was slightly thinner if the siRNA/EDA-CH_2CF_3-liposome (without freeze-thawing) was prepared in 1 mM citric acid. In addition, the band of siRNA was dramatically thinner after the 3 cycles of freeze-thawing of siRNA/EDA-CH_2CF_3-liposome in 1 mM citric acid. Free siRNA did not detected when EDA-CH_2CH_3-liposome was used regardless of the solution type or with/without freeze-thawing.

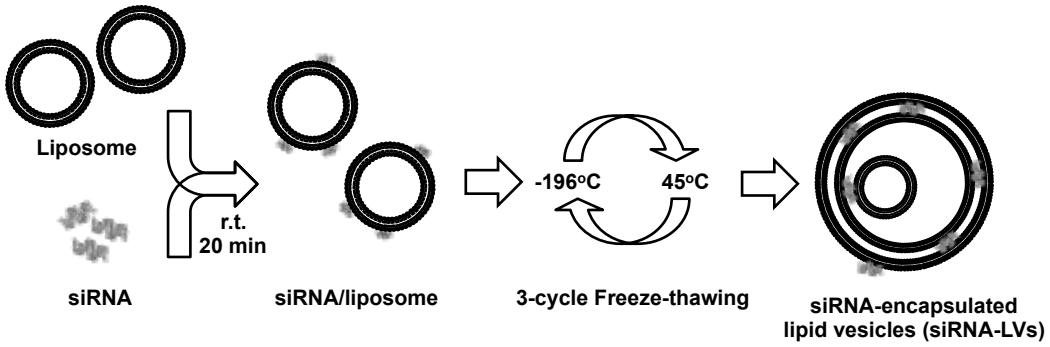

Scheme 2. Schematic image of preparation method for siRNA-encapsulated lipid vesicles

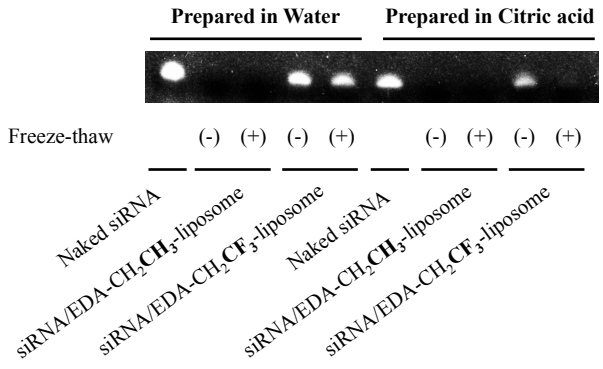

Figure 10. Preparation of siRNA-encapsulated lipid vesicles
After the preparation of 3-times freeze-thawed siRNA/liposome complex, free siRNA was separated by electrophoresis in a 15% acrylamide gel and stained with GelRed.

2-2-5. Cellular uptake and knockdown effect of siRNA-LVs-CPP

For *in vitro* experiments, cell-penetrating peptide (CPP) was modified on the siRNA-LVs surface (siRNA-LVs-CPP, **Scheme 3**). Uptake of siRNA into HT1080 cells was detected in each LVs (**Figure 11A**). Gene-silencing effect of each siRNA-LVs-CPP was determined using HT1080-EGFP cells (**Figure 11B**). In EDA-LVs, 39% of EGFP protein expression was suppressed by treatment with EDA-CH_2CH_3-LVs. Also, the amount of EGFP protein in the EDA-CH_2CH_2F- and EDA-CH_2CHF_2-LVs-treated cells was slightly reduced (approximately 25% reduction respectively). Little silencing effects were observed after treatment with EDA-CH_2CF_3-LVs. No cytotoxicity was observed in each siRNA-LVs-CPP (**Figure 11C**). Relative knockdown effect was shown as knockdown (%) / siRNA uptake (pmol/well) (**Figure 11D**). In DETA-LVs, DETA-CH_2CF_3-LVs-treated group showed the highest knockdown effect (50%). About 27% or 15% of knockdown effect were observed in DETA-CH_2CH_3-LVs- or DETA-CH_2CHF_2-LVs-treated group, respectively. DETA-CH_2CH_2F-LVs-treated group did not show the knockdown effect. DCP-EDA-CH_2CH_3 (pK_a = 8.2) -containing LVs-CPP showed high knockdown efficiency in the EDA library (mono-amine) and DCP-DETA-CH_2CF_3 (pK_{a1} = 7.1, pK_{a2} = < 3.0) -containing LVs-CPP showed high gene-silencing efficiency in the DETA library (di-amine).

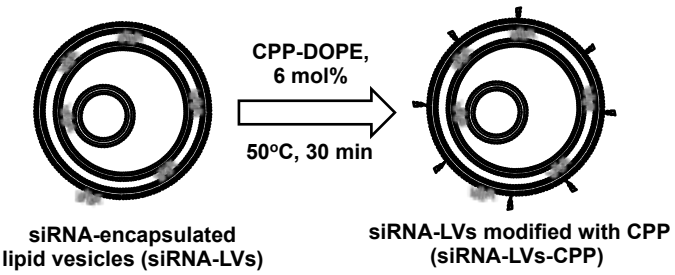

Scheme 3. Schematic image of siRNA-LVs-CPP

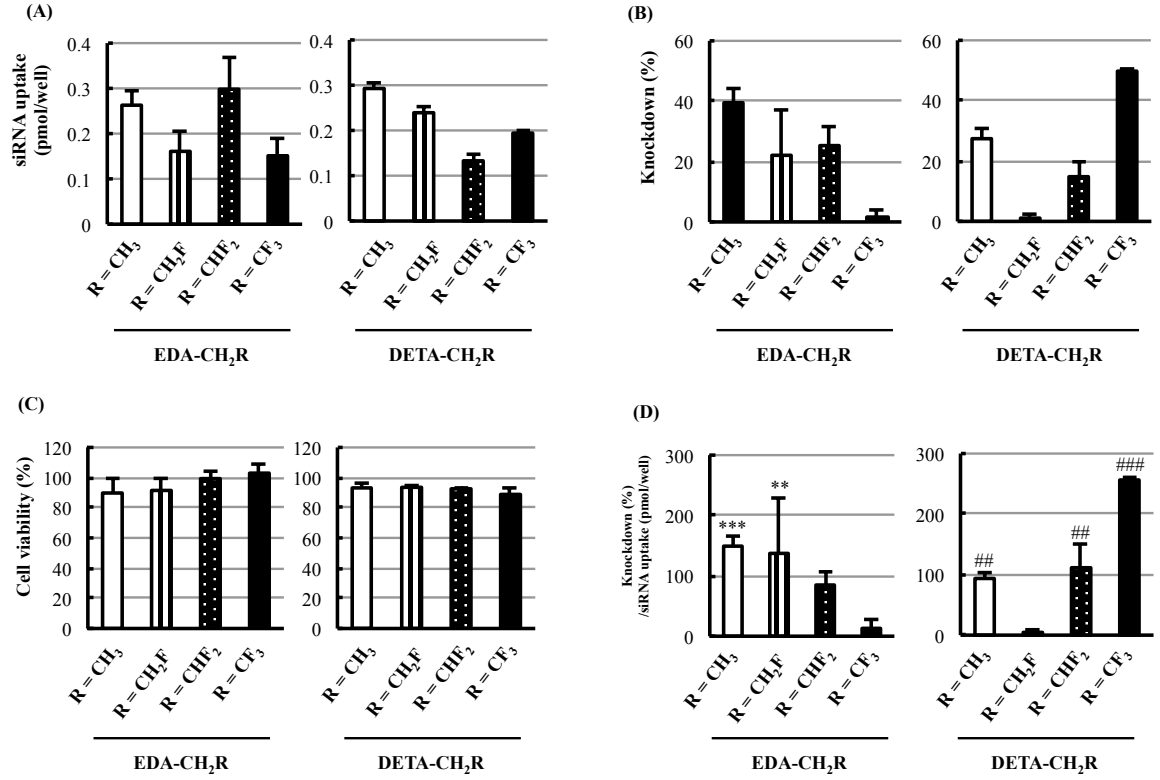

Figure 11. RNA interference effect of siRNA-LVs-CPP

(A) Cellular uptake of siRNA-LVs-CPP. HT1080 cells (1.5×10^4 cells/well) were lysed at 24 h after transfection of FITC-siRNA formulated in each LVs-CPP (5 pmol/500 μL; 10 nM as a siRNA concentration), and FITC intensity was measured. (B) Knockdown effect of siRNA-LVs-CPP. HT1080-EGFP cells (1.5×10^4 cells/well) were transfected with siRNA-LVs-CPP (5 pmol/100 μL; 10 nM as a siRNA concentration) for 24 h. After medium change, the cells were cultured for additional 48 h. Then, the cells were lysed and the fluorescence intensity of EGFP was measured. (C) Cell viability after transfection of siRNA-LVs-CPP. HT1080-EGFP cells were incubated with each sLVs-CPP for 24 h. After having been removed the medium, the cells were cultured for additional 48 h. Then, cell viability was determined by WST-8 assay. (D) RNA interference efficiency was determined as follows: Knockdown effect (%) / siRNA uptake (pmol/well). Symbols indicate significant differences (**P<0.01, ***P<0.001 *vs.* EDA-CH_2CF_3; $^{\#\#}P$<0.01 *vs.* DETA-CH_2CH_2F; $^{\#\#\#}P$<0.001 *vs.* DETA-CH_2CH_3, DETA-CH_2CH_2F and DETA- CH_2CHF_2).

2-2-6. Membrane-destabilizing activity of siRNA-LVs-CPP

To evaluate endosomal escape ability of each LV, hemolysis assay was performed. **Figure 12A** shows surface charge of the siRNA-LVs-CPP. Cow red blood cells were incubated with each siRNA-LVs-CPP in 10 mM phosphate buffer (pH 5.5 or pH 7.4) for 1 h. As a result, the pH-responsive hemolytic activity was observed in both of EDA- and DETA-LVs-CPP (**Figure 12B**). EDA-CH_2CH_3-LVs showed the highest membrane-damaging activity in the EDA-containing LVs; 34.9% at pH 7.4, 55.7% at pH 5.5. The hemolytic activity was decreased as the pK_a decreasing in the EDA-containing LVs-CPP. In contrast, the hemolytic activities were not significantly different in each DETA-containing LVs-CPP; ~10% at pH 7.4 and ~50% at pH 5.5.

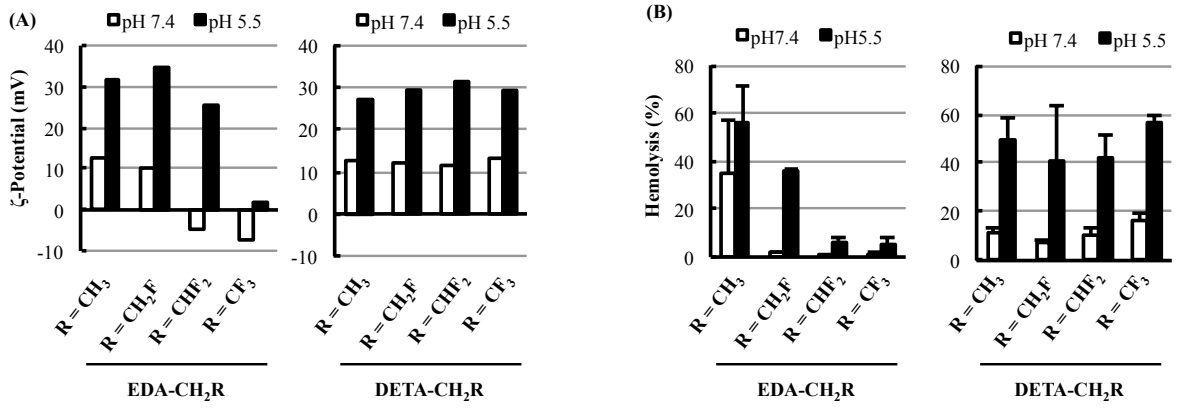

Figure 12. Membrane-destabilizing effect of siRNA-LVs-CPP

(A) Surface charge of siRNA-LVs-CPP. The ζ-potential of each siRNA-LVs-CPP in 10 mM phosphate buffer was measured. Bars with oblique line indicate the ζ-potentials of siRNA-LVs-CPP at pH 7.4. Filled bars indicate those at pH 5.5. (B) Hemolytic activity of siRNA-LVs-CPP against cow erythrocyte (RBCs). siRNA-LVs-CPP were incubated with RBCs at 37°C for 1 h in 10 mM phosphate buffer containing 0.3 M sucrose at pH 7.4 or 5.5. After centrifugation, absorbance of leaked-hemoglobin was determined at 405 nm.

2-2-7. Evaluation of interaction between siRNA and liposomes

To demonstrate binding affinity of siRNA for liposomes, apparent dissociation equilibrium constants (K_d) of siRNA for liposomes were measured by isothermal titration calorimetry (**Figure 13**, **Table 4**). The K_d of EDA-CH_2CH_3- or EDA-CH_2CH_2F-liposome at pH 7.4 was 1.27 μM or 2.43 μM, respectivery. The K_d of EDA-CH_2CHF_2- and EDA-CH_2CF_3-liposome were unable to determine. The K_d values of DETA-CH_2CH_3-, DETA-CH_2CH_2F-, or DETA-CH_2CHF_2-liposome were in the range of 100-500 nM at pH 7.4. In contrast, the K_d of DETA-CH_2CF_3-liposome was 3-10 times larger (1.57 μM) than that of other DETA-liposomes. siRNA showed stronger binding affinity for all DETA-liposomes at pH 5.5 (24-320 nM) than pH 7.4.

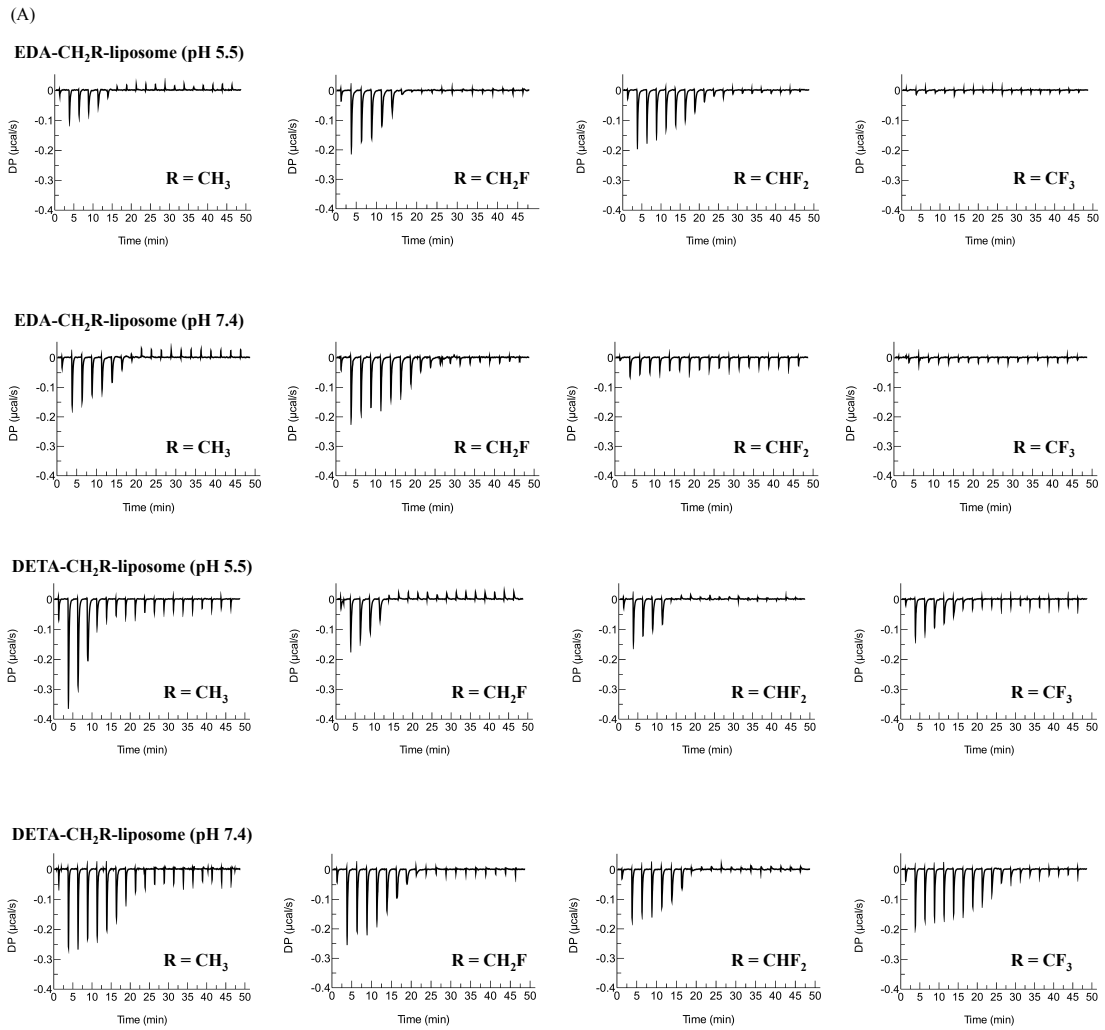

(B)

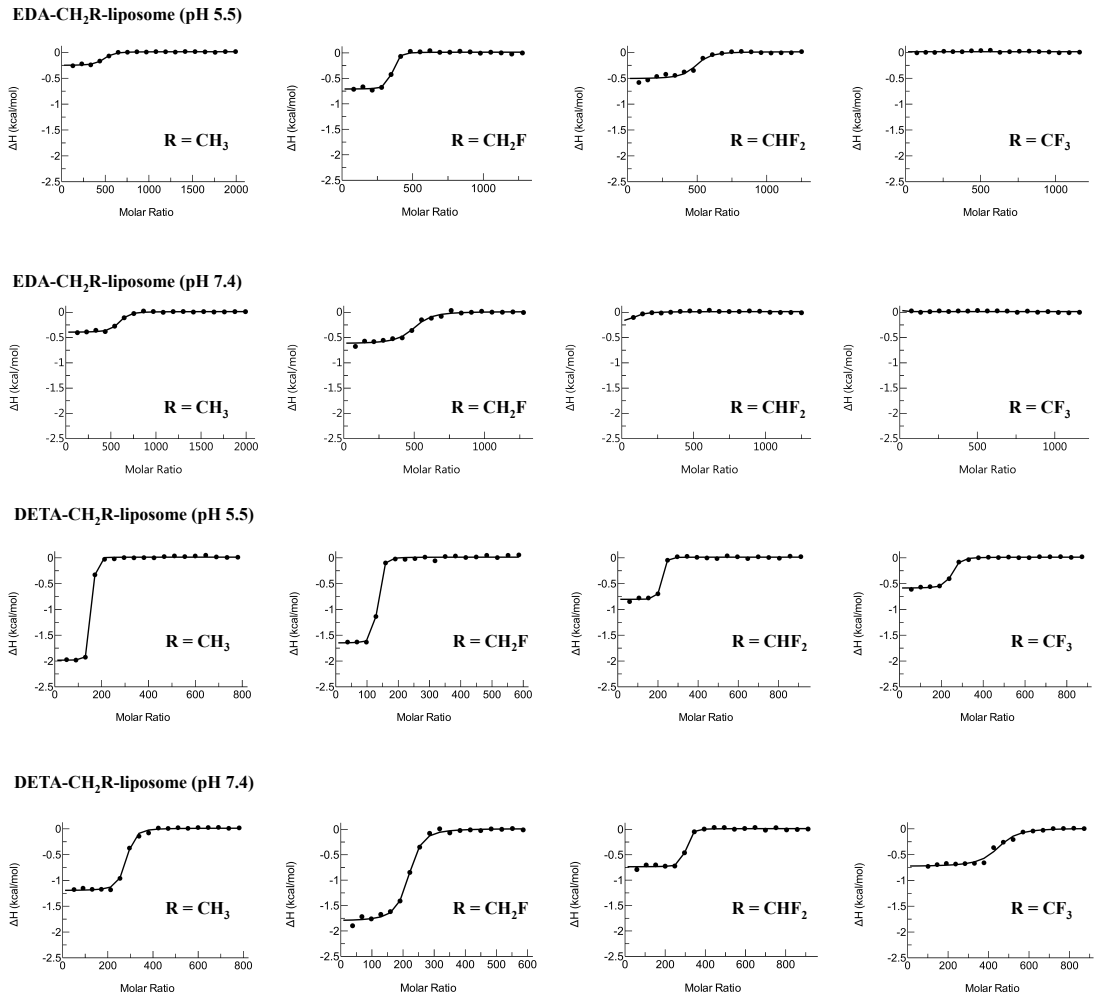

Figure 13. Interaction of siRNA with liposomes

EDA-liposome or DETA-liposome was titrated into the siRNA in 1 mM phosphate buffer at pH 7.4 or 5.5. Raw heat profile (A) and integrated curves (B) were determined using MicroCal PEAQ-ITC Analysis.

Table 4. K_d values of liposomes determined by ITC

EDA-CH_2R-liposome			DETA-CH_2R-liposome		
R	pH 7.4	pH 5.5	R	pH 7.4	pH 5.5
CH_3	1.27 μM	1.71 μM	CH_3	327 nM	24.3 nM
CH_2F	2.43 μM	273 nM	CH_2F	581 nM	75.0 nM
CHF_2	N.D.	1.58 μM	CHF_2	111 nM	41.6 nM
CF_3	N.D.	N.D.	CF_3	1.57 μM	320 nM

2-2-8. Intracellular distribution of FITC-siRNA

In order to investigate the intracellular behavior of siRNA, confocal laser-scanning microscopic time-lapse imaging was performed. FITC-conjugated siRNA was used for the experiment and each siRNA-LVs-CPP was transfected into HT1080 cells. siRNA releasing time into the cytoplasm (siRNA spreading throughout the cytoplasm) was recorded for the first 10 cells up to 24 h after the transfection (**Figure 14A**). EDA-CH_2CH_3-LVs-CPP showed the fastest siRNA release from LVs (2.94 hours) among the EDA-LVs. In contrast, DETA-CH_2CF_3-LVs-CPP did the fastest release of siRNA (2.05 hours) among the DETA-LVs. In addition, proportion of cells with siRNA-diffused throughout the cytoplasm at a selected time point was also different (**Figure 14B**). About 62% of cells were diffused siRNA at 24 h after the transfection by using EDA-CH_2CH_3-LVs-CPP. Similarly, about 76% of cells were diffused siRNA at 24 h by DETA-CH_2CF_3-LVs-CPP. However, portion of siRNA-diffused cells were less than 10% by using other LVs.

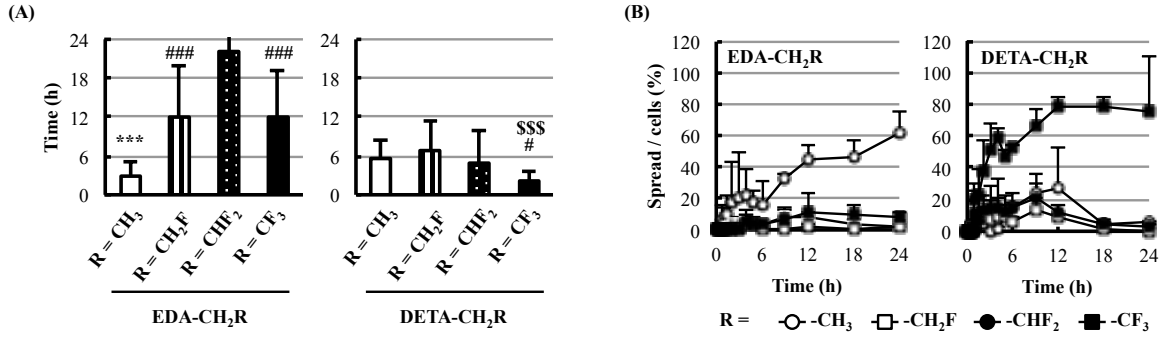

Figure 14. Intracellular behavior of siRNA delivered with LVs-CPP

HT1080 cells were seeded onto glass bottom 24-well plate (1.5×10^4 cells/well), and each LVs-CPP containing FITC-siRNA was added (10 nM; 5 pmol/500 μL as FITC-siRNA). Distribution of FITC-labeled siRNA and in the HT1080 cells was imaged over a 24-h period, with a 5-min shuttered interval. (A) siRNA diffusion time after transfection of LVs-CPP. Symbols indicate significant differences (***P<0.001 *vs.* EDA-CH_2CH_2F, EDA-CH_2CHF_2, and EDA-CH_2CF_3; $^{###}P$<0.001 *vs.* EDA-CH_2CHF_2; $^{\#}P$<0.05 *vs.* DETA-CH_2CH_3; $^{\$\$\$}P$<0.001 *vs.* DETA-$CH_2CH_2F$). (B) Proportion of siRNA-diffusing cell at selected time points. The ratio was calculated as follows: the number of FITC-distributed cells determined by FITC image / the number of all the cells determined by differential interference contrast image.

2-3. Discussion

Although several studies indicate that amine pK_a in the cationic part is one of the most important factors for the induction of highly efficient gene-silencing[60,62], amine pK_a has never been controlled without considerable change of chemical structure of cationic moiety. Hence, in this study, a small lipid library incorporating fluorine with DCP-EDA-CH_2R and DCP-DETA-CH_2R (R indicates: -CH_3, -CH_2F, -CHF_2 or -CF_3) was prepared (**Figure 7**). From pK_a measurement of each cationic-lipid with acid-base titration, it was revealed that the cationic-lipid pK_a was shifted to lower value by increasing the number of fluorine atoms (**Figure 8, Table 2**). pK_a of EDA-CH_2CF_3 and pK_{a2} of DETA-CH_2CF_3 could not determined because of the loss of buffering capacity at the range of pH 2–11. These results indicate that polyamine lipids having different responsibility for endosomal pH drop would be prepared. From these results, rigorous control of amine pK_a by fluorine substitution without significant change of chemical structure and steric bulk was succeeded.

Liposome containing EDA-CH_2CF_3 can be prepared when the lipid composition was DOPE / cholesterol / DPPC / EDA-CH_2CF_3 = 1/1/0.5/0.5 as a molar ratio (**Table 3**). Because trifluormethyl moiety is hydrophobic, EDA-CH_2CF_3-rich liposome should aggregate. The hydrophobicity might be eased with DPPC. Surface charge of each liposome (DOPE / cholesterol / DPPC / polyamine lipid = 1/1/0.5/0.5) was determined by TNS assay[69] (**Figure 9**). The result suggests that surface charge of mono-amine-containing nanoparticle depends on pK_a of amino group, however, that of di- or more amine-containing nanoparticle does not depend on the amine pK_a.

siRNA encapsulation after freeze-thawing was confirmed by electrophoretic assay. Free siRNA was not detected after the freeze-thawing of siRNA/EDA-CH_2CF_3-liposome in citric acid (**Figure 10**). On the other hand, freeze-thawing of the complex in water could not

prevent siRNA detaching from EDA-CH_2CF_3-liposome. These data suggested that the siRNA was not strongly attached to the liposome surface in water where the electrostatic interaction was not strong enough to hold the siRNA. Surface potential of EDA-CH_2CF_3 liposome in water and 1 mM citric acid (pH 3.05) was determined as +8.52 mV and +55.5 mV, respectively. Previously, it was reported that the increase of siRNA-encapsulating capacity by freeze-thawing was observed in liposomes with cationic surface charge, but not in liposomes with neutral surface charge[68]. Therefore, cationic-charged EDA-CH_2CF_3-liposome could hold siRNA during freeze-thawing in citric acid. Hence, in this study, siRNA-encapsulated lipid vesicles (siRNA-LVs) using various polyamine lipids were prepared in 1 mM citric acid.

Then, to determine the RNA interference efficiency of siRNA-LVs, siRNA uptake and gene silencing effect was determined. As preparatory experiment, each LVs encapsulating FITC-labeled siRNA was added to HT1080 cells to demonstrate the siRNA uptake into the cells at 24 h after the transfection. Increasing fluorine atom number into the amine group tends to decrease siRNA uptake (data not shown). There was a great difference of siRNA uptake between the maximum and minimum value (~10 times). If the difference in siRNA amount in the cells is too large, gene-silencing effects might not be compared appropriately. Therefore, equalization of siRNA uptake into the cell appears to be important in this study. Modification of functional peptides has often used to improve cellular uptake of nanocarriers[70]. To equalize siRNA uptake, siRNA-encapsulated lipid vesicles were modified with cell-penetrating peptide (siRNA-LVs-CPP) for *in vitro* use (**Scheme 3**). siRNA uptake was between 0.13 pmol/well to 0.30 pmol/well among all LVs modified with CPP (**Figure 11A**). From the data of cellular uptake and knockdown effect, RNA interference efficiency of siRNA was determined (**Figure 11D**). Surprisingly, optimal amine pK_a for high knockdown effect depended on the number of amine. These results indicate that the balance between the numbers of amine and fluorine atoms is crucial to achieve the high knockdown effect.

To evaluate membrane-destabilizing activity of these cationic lipid-containing liposomes, hemolysis assay was performed. It is known that endosomal escape ability is important for the gene-silencing induction[51,71]. RBC hemolysis assay is known as a surrogate assay for endosomal escape ability test because of similarities in their lipid bilayer and glycocalyx compositions[72]. As endosomal pH is known to be decreasing with endosome maturation[73], RBC was incubated with each sLVs-CPP in 10 mM phosphate buffer (pH 5.5 or 7.4) for 1 h. As shown in **Figure 12**, pH-responsive hemolytic activity was observed in both of EDA and DETA libraries. It is known that the positively charged nanoparticles tend to induce strong hemolytic activity[74]. Since the surface charge of siRNA-EDA-LVs-CPP decreased with the fluorine number increasing (**Figure 12A**), hemolytic activity should be also decreased accordingly (**Figure 12B**). These results indicate that EDA-CH_2CHF_2- and EDA-CH_2CF_3-LVs could not break the endosomal membrane even if the endosome was acidified. Then, the siRNA should stay in endosome and be enzymatically degraded[75]. Therefore, siRNA delivered with EDA-CH_2CHF_2- and EDA-CH_2CF_3-LVs-CPP barely showed gene-silencing effect in **Figure 11**. In contrast, there was no correlation between the number of fluorine atoms and the hemolytic activity in DETA library. Surface charges of siRNA-DETA-LVs-CPP were not significantly changed even if increasing of fluorine atom number because pK_{a2} is still above 5.5. Therefore, hemolytic activities of siRNA-DETA-LVs-CPP were not changed with the fluorine atom number unlike EDA-LVs. The data suggest that impact of pK_a on membrane-destabilizing activity would be not large in the di- or more- amine-containing LVs.

siRNA needs to form RISC in cytoplasm after the endosomal escape for gene-silencing. Therefore, effective hand-off of siRNA from LVs to the RISC is important for strong gene-silencing. It was hypothesized that binding affinity of siRNA for DETA-CH_2CF_3 liposomes would be weak in the cytoplasm compared with other DETA liposomes. **Figure 13**

and **Table 4** shows the binding affinity of siRNA for liposomes measured by isothermal titration calorimetry. It was found that liposome containing DETA-CH_2CF_3 showed remarkably weak interaction with siRNA at pH 7.4 (K_d = 1.57 μM) among with DETA-lipid-containing liposomes. Since the pK_a of DCP-DETA-CH_2CF_3 is lower (pK_{a1} = 7.1, pK_{a2} < 3.0) than those of other DETA-lipids, amine of the DETA-CH_2CF_3-liposomes should be less protonated than other DETA-liposome at pH 7.4. As shown in **Figure 12B**, each DETA-LVs-CPP had equal hemolytic activity. Therefore, it was hypothesized that weak interaction of siRNA for liposomes in the cytoplasm i.e. release of siRNA from liposomes should be important for strong gene silencing effect.

To examine the hypothesis, siRNA release time into the cytoplasm from LVs was measured by time-lapse imaging using confocal laser scanning microscope (**Figure 14A**). EDA-CH_2CH_3- and DETA-CH_2CF_3-LVs-CPP showed faster siRNA release from LVs than other LVs-CPP. In addition, the diffusion of siRNA was observed in about 70% of cells 24 h after the transfection by using EDA-CH_2CH_3- and DETA-CH_2CF_3-LVs-CPP (**Figure 14B**). As DCP-EDA-CH_2CH_3 has a pK_a of 8.2 and the LVs has a positively charged surface, it seems that it could escape from endosome mainly by electrostatic interaction. After the entrance to the cytoplasm, electrostatic interaction with siRNA should have remained even in the environment of pH 7.4. However, since the interaction of siRNA to liposome containing EDA-CH_2CH_3 is weak (K_d = 1.27 μM), it should be difficult to retain the siRNA on the liposome. On the other hand, liposomes containing DCP-EDA-CH_2CH_2F (pK_a = 5.3), DCP-EDA-CH_2CHF_2 (pK_a = 4.4) or DCP-EDA-CH_2CF_3 (pK_a < 3.3) seemed to be difficult to escape from endosomes because of low pK_a. Therefore, the diffusion of siRNA might not be observed. In terms of DETA-series, it seems that every DETA-LVs can escape from the endosome because they have positively charged surface. However, as shown in **Table 4**, affinity of siRNA for liposome containing DETA-CH_2CF_3 was relatively weak (K_d = 1.57

μM) at pH 7.4 compared with other DETA-liposomes. Therefore, the DETA-CH_2CF_3-liposome can release siRNA to all over the cytoplasm effectively after the endosomal escape. On the other hand, other DETA-liposomes could not diffuse siRNA into the cytoplasm due to the strong interaction with siRNA.

Part 2. - Conclusion

In conclusion, rigorous control of amine pK_a by fluorine substitution without significant change of chemical structure and steric bulk. Optimal amine pK_a for the efficient gene-silencing depended on the number of amine. Liposomes that showed high RNA interference efficiency might be superior in cytoplasmic release of siRNA. In addition, it was revealed that the binding affinity of siRNA to the carriers changes even if the cationic carriers show similar properties including surface charge, hemolytic activity. Moderate interaction between siRNA and nanocarrier was important for effective gene-silencing. These results indicate that it is important to control pK_a of the carrier accurately and to evaluate whether the pK_a brings desired interaction to achieve the ideal multifunctionalitiy of the vector.

Afterword

In this study, it was demonstrated that improvement of siRNA delivery to target site is achievable by adding desirable functions to lipid nanoparticles. Since siRNA is a promising drug candidate for satisfying unmet medical needs, the development of innovative DDS technology is absolutely required. Advanced research on lipid nanoparticle-based drugs would contribute to establish healthy longevity society with high quality of life. I hope that this research contributes to advancement of siRNA drug development.

Acknowledgement

This dissertation is a report that was carried out at Department of Medical Biochemistry, University of Shizuoka Graduate School of Pharmaceutical Sciences.

I would like to express my sincere gratitude to my supervisor, Professor Naoto Oku for providing me this precious study opportunity as a Ph.D. student in his laboratory and supporting my school life. I am deeply grateful to my supervisors, Dr. Tomohiro Asai, Dr. Hiroyuki Koide, Dr. Kosuke Shimizu, and Dr. Junko Kimura for their elaborated guidance, considerable encouragements, and valuable discussions. I also thank Associate Professor Philip Hawke of the University of Shizuoka Scientific English Program for the English editing. I very much appreciate all laboratory members at the Department of Medical Biochemistry for my unforgettable school life.

I greatly acknowledge Prof. Tetsuo Minamino at the Department of Cardiorenal and Cerebrovascular Medicine, Kagawa University Faculty of Medicine, and Prof Emer. Eisuke Mekada at the Research Institute for Microbial Diseases, Osaka University for the gift of HB-EGF IgG. I also deeply thank Mr. Naoki Morita and Prof. Yoshitaka Hamashima for synthesis of fluorine-conjugated lipids. I greatly appreciate Prof. Yoshiyuki Kagawa, Prof. Satomi Onoue and Prof. Shigeru Itai for helpful discussions and suggestions. I am very grateful to Mr. Furan Song, Mr. Masafumi Yokota, Mr. Sho Ryu, Mr. Noriaki Okada, Mr. Hideki Isomura, Mr. Masahiro Hashimoto, Ms. Mariko Sako, Mr. Naoyuki Sakurai, Mr. Yusuke Hirai and Ms. Ryoko Saeki for their valuable supports in my experiments. I am deeply grateful to Mr. Hiroki Kato, Mr. Shoya Takahashi, Dr. Hidenori Ando, Dr. Jantana Yahuafai, Dr. Tatsuya Fukuta, and Dr. Takayuki Ishii for teaching me the basis of experiment and research life. I am also very thankful to the Japan Society for the Promotion of Science for making my Ph.D. study possible by the financial support. Finally, I am really thankful to my family for their understanding of my study, support and encouragement.

March 2018

Ayaka Okamoto

References

[1] Fire, A.; Xu, S.; Montgomery, M. K.; Kostas, S. A.; Driver, S. E.; Mello, C. C. Potent and specific genetic interference by double-stranded RNA in Caenorhabditis elegans. *Nature* **1998,** *391*, 806.

[2] Zamore, P. D.; Tuschl, T.; Sharp, P. A.; Bartel, D. P. RNAi: double-stranded RNA directs the ATP-dependent cleavage of mRNA at 21 to 23 nucleotide intervals. *Cell* **2000,** *101*, 25.

[3] Morrissey, D. V.; Lockridge, J. A.; Shaw, L.; Blanchard, K.; Jensen, K.; Breen, W.; Hartsough, K.; Machemer, L.; Radka, S.; Jadhav, V.; Vaish, N.; Zinnen, S.; Vargeese, C.; Bowman, K.; Shaffer, C. S.; Jeffs, L. B.; Judge, A.; MacLachlan, I.; Polisky, B. Potent and persistent in vivo anti-HBV activity of chemically modified siRNAs. *Nature biotechnology* **2005,** *23*, 1002.

[4] Whitehead, K. A.; Langer, R.; Anderson, D. G. Knocking down barriers: advances in siRNA delivery. *Nat Rev Drug Discov* **2009,** *8*, 129.

[5] Akita, H.; Kudo, A.; Minoura, A.; Yamaguti, M.; Khalil, I. A.; Moriguchi, R.; Masuda, T.; Danev, R.; Nagayama, K.; Kogure, K.; Harashima, H. Multi-layered nanoparticles for penetrating the endosome and nuclear membrane via a step-wise membrane fusion process. *Biomaterials* **2009,** *30*, 2940.

[6] Belliveau, N. M.; Huft, J.; Lin, P. J.; Chen, S.; Leung, A. K.; Leaver, T. J.; Wild, A. W.; Lee, J. B.; Taylor, R. J.; Tam, Y. K.; Hansen, C. L.; Cullis, P. R. Microfluidic Synthesis of Highly Potent Limit-size Lipid Nanoparticles for In Vivo Delivery of siRNA. *Mol Ther Nucleic Acids* **2012,** *1*, e37.

[7] Somiya, M.; Yamaguchi, K.; Liu, Q.; Niimi, T.; Maturana, A. D.; Iijima, M.; Yoshimoto, N.; Kuroda, S. One-step scalable preparation method for non-cationic liposomes with high siRNA content. *International journal of pharmaceutics* **2015,** *490*, 316.

[8] http://investors.alnylam.com/news-releases/news-release-details/european-medicines-agency-ema-grants-alnylam-accelerated (Press Release from Alnylam on Nov. 13, 2017)

[9] Kaczmarek, J. C.; Kowalski, P. S.; Anderson, D. G. Advances in the delivery of RNA therapeutics: from concept to clinical reality. *Genome Med* **2017,** *9*, 60.

[10] World health statistics 2017: monitoring health for the SDGs, Sustainable Development Goals. Geneva: World Health Organization; **2017**. Licence: CC BY-NC-SA 3.0 IGO. (URL: http://apps.who.int/iris/bitstream/10665/255336/1/9789241565486-eng.pdf)

[11] Vital Statistics: Statistics and Information Department. Ministry of Health, Labour and Welfare; **2017**

[12] Perou, C. M.; Sorlie, T.; Eisen, M. B.; van de Rijn, M.; Jeffrey, S. S.; Rees, C. A.; Pollack, J. R.; Ross, D. T.; Johnsen, H.; Akslen, L. A.; Fluge, O.; Pergamenschikov, A.; Williams, C.; Zhu, S. X.; Lonning, P. E.; Borresen-Dale, A. L.; Brown, P. O.; Botstein, D. Molecular portraits of human breast tumours. *Nature* **2000,** *406*, 747.

[13] Bauer, K. R.; Brown, M.; Cress, R. D.; Parise, C. A.; Caggiano, V. Descriptive analysis of estrogen receptor (ER)-negative, progesterone receptor (PR)-negative, and HER2-negative invasive breast cancer, the so-called triple-negative phenotype: a population-based study from the California cancer Registry. *Cancer* **2007,** *109*, 1721.

[14] Shen, J.; Liu, H.; Mu, C.; Wolfram, J.; Zhang, W.; Kim, H. C.; Zhu, G.; Hu, Z.; Ji, L. N.; Liu, X.; Ferrari, M.; Mao, Z. W.; Shen, H. Multi-step encapsulation of chemotherapy and gene silencing agents in functionalized mesoporous silica nanoparticles. *Nanoscale* **2017,** *9*, 5329.

[15] Sarett, S. M.; Werfel, T. A.; Lee, L.; Jackson, M. A.; Kilchrist, K. V.; Brantley-Sieders, D.; Duvall, C. L. Lipophilic siRNA targets albumin in situ and promotes bioavailability, tumor penetration, and carrier-free gene silencing. *Proc Natl Acad Sci U S A* **2017**.

[16] Parmar, M. B.; Arteaga Ballesteros, B. E.; Fu, T.; K, C. R.; Montazeri Aliabadi, H.; Hugh, J. C.; Lobenberg, R.; Uludag, H. Multiple siRNA delivery against cell cycle and anti-apoptosis proteins using lipid-substituted polyethylenimine in triple-negative breast cancer and nonmalignant cells. *J Biomed Mater Res A* **2016,** *104*, 3031.

[17] Yang, Z.; Liu, T.; Xie, Y.; Sun, Z.; Liu, H.; Lin, J.; Liu, C.; Mao, Z. W.; Nie, S. Chitosan layered gold nanorods as synergistic therapeutics for photothermal ablation and gene silencing in triple-negative breast cancer. *Acta Biomater* **2015,** *25*, 194.

[18] Liu, Y.; Zhu, Y. H.; Mao, C. Q.; Dou, S.; Shen, S.; Tan, Z. B.; Wang, J. Triple negative breast cancer therapy with CDK1 siRNA delivered by cationic lipid assisted PEG-PLA nanoparticles. *Journal of controlled release* **2014,** *192*, 114.

[19] Parvani, J. G.; Gujrati, M. D.; Mack, M. A.; Schiemann, W. P.; Lu, Z. R. Silencing beta3 Integrin by Targeted ECO/siRNA Nanoparticles Inhibits EMT and Metastasis of Triple-Negative Breast Cancer. *Cancer Res* **2015,** *75*, 2316.

[20] Iwamoto, R.; Mekada, E. ErbB and HB-EGF signaling in heart development and function. *Cell Struct Funct* **2006,** *31*, 1.

[21] Minami, S.; Iwamoto, R.; Mekada, E. HB-EGF decelerates cell proliferation synergistically with TGFalpha in perinatal distal lung development. *Dev Dyn* **2008,** *237*, 247.

[22] Yahata, Y.; Shirakata, Y.; Tokumaru, S.; Yang, L.; Dai, X.; Tohyama, M.; Tsuda, T.; Sayama, K.; Iwai, M.; Horiuchi, M.; Hashimoto, K. A novel function of angiotensin II in skin wound healing. Induction of fibroblast and keratinocyte migration by angiotensin II via heparin-binding epidermal growth factor (EGF)-like growth factor-mediated EGF receptor transactivation. *J Biol Chem* **2006,** *281*, 13209.

[23] Yotsumoto, F.; Yagi, H.; Suzuki, S. O.; Oki, E.; Tsujioka, H.; Hachisuga, T.; Sonoda, K.; Kawarabayashi, T.; Mekada, E.; Miyamoto, S. Validation of HB-EGF and amphiregulin as targets for human cancer therapy. *Biochemical and biophysical research communications* **2008,** *365*, 555.

[24] Lin, A.; Li, C.; Xing, Z.; Hu, Q.; Liang, K.; Han, L.; Wang, C.; Hawke, D. H.; Wang, S.; Zhang, Y.; Wei, Y.; Ma, G.; Park, P. K.; Zhou, J.; Zhou, Y.; Hu, Z.; Zhou, Y.; Marks, J. R.; Liang, H.; Hung, M. C.; Lin, C.; Yang, L. The LINK-A lncRNA activates normoxic HIF1alpha signalling in triple-negative breast cancer. *Nat Cell Biol* **2016,** *18*, 213.

[25] Yotsumoto, F.; Tokunaga, E.; Oki, E.; Maehara, Y.; Yamada, H.; Nakajima, K.; Nam, S. O.; Miyata, K.; Koyanagi, M.; Doi, K.; Shirasawa, S.; Kuroki, M.; Miyamoto, S. Molecular hierarchy of heparin-binding EGF-like growth factor-regulated angiogenesis in triple-negative breast cancer. *Mol Cancer Res* **2013,** *11*, 506.

[26] Kuo, P. L.; Huang, M. S.; Hung, J. Y.; Chou, S. H.; Chiang, S. Y.; Huang, Y. F.; Yang, C. J.; Tsai, M. J.; Chang, W. A.; Hsu, Y. L. Synergistic effect of lung tumor-associated dendritic cell-derived HB-EGF and CXCL5 on cancer progression. *Int J Cancer* **2014,** *135*, 96.

[27] Yotsumoto, F.; Oki, E.; Tokunaga, E.; Maehara, Y.; Kuroki, M.; Miyamoto, S. HB-EGF orchestrates the complex signals involved in triple-negative and trastuzumab-resistant breast cancer. *Int J Cancer* **2010,** *127*, 2707.

[28] Nam, S. O.; Yotsumoto, F.; Miyata, K.; Fukagawa, S.; Odawara, T.; Manabe, S.; Ishikawa, T.; Kuroki, M.; Yasunaga, S.; Miyamoto, S. Anti-tumor Effect of Intravenous Administration of CRM197 for Triple-negative Breast Cancer Therapy. *Anticancer Res* **2016,** *36*, 3651.

[29] Agarwal, M.; Sahoo, A. K.; Bose, B. Receptor-Mediated Enhanced Cellular Delivery of Nanoparticles Using Recombinant Receptor-Binding Domain of Diphtheria Toxin. *Mol Pharm* **2017,** *14*, 23.

[30] Liu, X.; Erikson, R. L. Polo-like kinase (Plk)1 depletion induces apoptosis in cancer cells. *Proc Natl Acad Sci U S A* **2003,** *100*, 5789.

[31] Luo, J.; Emanuele, M. J.; Li, D.; Creighton, C. J.; Schlabach, M. R.; Westbrook, T. F.; Wong, K. K.; Elledge, S. J. A genome-wide RNAi screen identifies multiple synthetic lethal interactions with the Ras oncogene. *Cell* **2009,** *137*, 835.

[32] Brenner, J. C.; Ateeq, B.; Li, Y.; Yocum, A. K.; Cao, Q.; Asangani, I. A.; Patel, S.; Wang, X.; Liang, H.; Yu, J.; Palanisamy, N.; Siddiqui, J.; Yan, W.; Cao, X.; Mehra, R.; Sabolch, A.; Basrur, V.; Lonigro, R. J.; Yang, J.; Tomlins, S. A.; Maher, C. A.; Elenitoba-Johnson, K. S.; Hussain, M.; Navone, N. M.; Pienta, K. J.; Varambally, S.; Feng, F. Y.; Chinnaiyan, A. M. Mechanistic rationale for inhibition of poly(ADP-ribose) polymerase in ETS gene fusion-positive prostate cancer. *Cancer Cell* **2011,** *19*, 664.

[33] Mishra, A.; Liu, S.; Sams, G. H.; Curphey, D. P.; Santhanam, R.; Rush, L. J.; Schaefer, D.; Falkenberg, L. G.; Sullivan, L.; Jaroncyk, L.; Yang, X.; Fisk, H.; Wu, L. C.; Hickey, C.; Chandler, J. C.; Wu, Y. Z.; Heerema, N. A.; Chan, K. K.; Perrotti, D.; Zhang, J.; Porcu, P.; Racke, F. K.; Garzon, R.; Lee, R. J.; Marcucci, G.; Caligiuri, M. A. Aberrant overexpression of IL-15 initiates large granular lymphocyte leukemia through chromosomal instability and DNA hypermethylation. *Cancer Cell* **2012,** *22*, 645.

[34] Hamaoka, M.; Chinen, I.; Murata, T.; Takashima, S.; Iwamoto, R.; Mekada, E. Anti-human HB-EGF monoclonal antibodies inhibiting ectodomain shedding of HB-EGF and diphtheria toxin binding. *J Biochem* **2010,** *148*, 55.

[35] Nishikawa, K.; Asai, T.; Shigematsu, H.; Shimizu, K.; Kato, H.; Asano, Y.; Takashima, S.; Mekada, E.; Oku, N.; Minamino, T. Development of anti-HB-EGF immunoliposomes for the treatment of breast cancer. *Journal of controlled release* **2012,** *160*, 274.

[36] Estep, P.; Reid, F.; Nauman, C.; Liu, Y.; Sun, T.; Sun, J.; Xu, Y. High throughput solution-based measurement of antibody-antigen affinity and epitope binning. *MAbs* **2013,** *5*, 270.

[37] Bhattacharyya, S.; Bhattacharya, R.; Curley, S.; McNiven, M. A.; Mukherjee, P. Nanoconjugation modulates the trafficking and mechanism of antibody induced receptor endocytosis. *Proc Natl Acad Sci U S A* **2010,** *107*, 14541.

[38] Dou, S.; Yao, Y. D.; Yang, X. Z.; Sun, T. M.; Mao, C. Q.; Song, E. W.; Wang, J. Anti-Her2 single-chain

antibody mediated DNMTs-siRNA delivery for targeted breast cancer therapy. *Journal of controlled release* **2012,** *161*, 875.

[39] Matsumura, Y.; Maeda, H. A new concept for macromolecular therapeutics in cancer chemotherapy: mechanism of tumoritropic accumulation of proteins and the antitumor agent smancs. *Cancer Res* **1986,** *46*, 6387.

[40] Mamot, C.; Drummond, D. C.; Greiser, U.; Hong, K.; Kirpotin, D. B.; Marks, J. D.; Park, J. W. Epidermal growth factor receptor (EGFR)-targeted immunoliposomes mediate specific and efficient drug delivery to EGFR- and EGFRvIII-overexpressing tumor cells. *Cancer Res* **2003,** *63*, 3154.

[41] Kimura, A.; Terao, M.; Kato, A.; Hanafusa, T.; Murota, H.; Katayama, I.; Miyoshi, E. Upregulation of N-acetylglucosaminyltransferase-V by heparin-binding EGF-like growth factor induces keratinocyte proliferation and epidermal hyperplasia. *Exp Dermatol* **2012,** *21*, 515.

[42] Hieda, M.; Koizumi, M.; Higashi, C.; Tachibana, T.; Taguchi, T.; Higashiyama, S. The cytoplasmic tail of heparin-binding EGF-like growth factor regulates bidirectional intracellular trafficking between the plasma membrane and ER. *FEBS Open Bio* **2012,** *2*, 339.

[43] Mochizuki, S.; Kanegae, N.; Nishina, K.; Kamikawa, Y.; Koiwai, K.; Masunaga, H.; Sakurai, K. The role of the helper lipid dioleoylphosphatidylethanolamine (DOPE) for DNA transfection cooperating with a cationic lipid bearing ethylenediamine. *Biochim Biophys Acta* **2013,** *1828*, 412.

[44] Sun, W.; Su, Q.; Cao, X.; Shang, B.; Chen, A.; Yin, H.; Liu, B. High expression of polo-like kinase 1 is associated with early development of hepatocellular carcinoma. *Int J Genomics* **2014,** *2014*, 312130.

[45] Pellegrino, R.; Calvisi, D. F.; Ladu, S.; Ehemann, V.; Staniscia, T.; Evert, M.; Dombrowski, F.; Schirmacher, P.; Longerich, T. Oncogenic and tumor suppressive roles of polo-like kinases in human hepatocellular carcinoma. *Hepatology* **2010,** *51*, 857.

[46] Kiso, S.; Kawata, S.; Tamura, S.; Ito, N.; Tsushima, H.; Yamada, A.; Higashiyama, S.; Taniguchi, N.; Matsuzawa, Y. Expression of heparin-binding EGF-like growth factor in rat liver injured by carbon tetrachloride or D-galactosamine. *Biochemical and biophysical research communications* **1996,** *220*, 285.

[47] Ikeda, S.; Neyts, J.; Matsuura, M.; Kiso, M.; Hasegawa, A.; Nishimura, C.; De Clercq, E. Protective activity of the lipid A analogue GLA-60 against murine cytomegalovirus infection in immunodeficient mice. *J Gen Virol* **1993,** *74*, 1399.

[48] Bae, Y. H.; Park, K. Targeted drug delivery to tumors: myths, reality and possibility. *Journal of controlled release* **2011,** *153*, 198.

[49] Gibby, K.; You, W. K.; Kadoya, K.; Helgadottir, H.; Young, L. J.; Ellies, L. G.; Chang, Y.; Cardiff, R. D.; Stallcup, W. B. Early vascular deficits are correlated with delayed mammary tumorigenesis in the MMTV-PyMT transgenic mouse following genetic ablation of the NG2 proteoglycan. *Breast Cancer Res* **2012,** *14*, R67.

[50] Murata, T.; Mizushima, H.; Chinen, I.; Moribe, H.; Yagi, S.; Hoffman, R. M.; Kimura, T.; Yoshino, K.; Ueda, Y.; Enomoto, T.; Mekada, E. HB-EGF and PDGF mediate reciprocal interactions of carcinoma cells with cancer-associated fibroblasts to support progression of uterine cervical cancers. *Cancer Res* **2011,** *71*, 6633-42.

[51] Dowdy, S. F. Overcoming cellular barriers for RNA therapeutics. *Nature biotechnology* **2017,** *35*, 222.

[52] Dewa, T.; Asai, T.; Tsunoda, Y.; Kato, K.; Baba, D.; Uchida, M.; Sumino, A.; Niwata, K.; Umemoto, T.; Iida, K.; Oku, N.; Nango, M. Liposomal polyamine-dialkyl phosphate conjugates as effective gene carriers: chemical structure, morphology, and gene transfer activity. *Bioconjug Chem* **2010,** *21*, 844.

[53] Semple, S. C.; Klimuk, S. K.; Harasym, T. O.; Dos Santos, N.; Ansell, S. M.; Wong, K. F.; Maurer, N.; Stark, H.; Cullis, P. R.; Hope, M. J.; Scherrer, P. Efficient encapsulation of antisense oligonucleotides in lipid vesicles using ionizable aminolipids: formation of novel small multilamellar vesicle structures. *Biochim Biophys Acta* **2001,** *1510*, 152.

[54] Bartlett, D. W.; Davis, M. E. Physicochemical and biological characterization of targeted, nucleic acid-containing nanoparticles. *Bioconjug Chem* **2007,** *18*, 456.

[55] Ghosn, B.; Kasturi, S. P.; Roy, K. Enhancing polysaccharide-mediated delivery of nucleic acids through functionalization with secondary and tertiary amines. *Curr Top Med Chem* **2008,** *8*, 331.

[56] Toita, S.; Morimoto, N.; Akiyoshi, K. Functional cycloamylose as a polysaccharide-based biomaterial: application in a gene delivery system. *Biomacromolecules* **2010,** *11*, 397.

[57] Boussif, O.; Lezoualc'h, F.; Zanta, M. A.; Mergny, M. D.; Scherman, D.; Demeneix, B.; Behr, J. P. A versatile vector for gene and oligonucleotide transfer into cells in culture and in vivo: polyethylenimine. *Proc Natl Acad Sci U S A* **1995,** *92*, 7297.

[58] Moghimi, S. M.; Symonds, P.; Murray, J. C.; Hunter, A. C.; Debska, G.; Szewczyk, A. A two-stage poly(ethylenimine)-mediated cytotoxicity: implications for gene transfer/therapy. *Mol Ther* **2005,** *11*, 990.

[59] Uchida, H.; Miyata, K.; Oba, M.; Ishii, T.; Suma, T.; Itaka, K.; Nishiyama, N.; Kataoka, K. Odd-even effect of repeating aminoethylene units in the side chain of N-substituted polyaspartamides on gene transfection profiles. *J Am Chem Soc* **2011,** *133*, 15524.

[60] Jayaraman, M.; Ansell, S. M.; Mui, B. L.; Tam, Y. K.; Chen, J.; Du, X.; Butler, D.; Eltepu, L.; Matsuda, S.; Narayanannair, J. K.; Rajeev, K. G.; Hafez, I. M.; Akinc, A.; Maier, M. A.; Tracy, M. A.; Cullis, P. R.; Madden, T. D.; Manoharan, M.; Hope, M. J. Maximizing the potency of siRNA lipid nanoparticles for hepatic gene silencing in vivo. *Angew Chem Int Ed Engl* **2012,** *51*, 8529.

[61] Alabi, C. A.; Love, K. T.; Sahay, G.; Yin, H.; Luly, K. M.; Langer, R.; Anderson, D. G. Multiparametric approach for the evaluation of lipid nanoparticles for siRNA delivery. *Proc Natl Acad Sci U S A* **2013,** *110*, 12881.

[62] Sato, Y.; Hatakeyama, H.; Hyodo, M.; Harashima, H. Relationship Between the Physicochemical Properties of Lipid Nanoparticles and the Quality of siRNA Delivery to Liver Cells. *Mol Ther* **2016,** *24*, 788.

[63] Hao, J.; Kos, P.; Zhou, K.; Miller, J. B.; Xue, L.; Yan, Y.; Xiong, H.; Elkassih, S.; Siegwart, D. J. Rapid Synthesis of a Lipocationic Polyester Library via Ring-Opening Polymerization of Functional Valerolactones for Efficacious siRNA Delivery. *J Am Chem Soc* **2015,** *137*, 9206.

[64] Dunitz, J. D.; Gavezzotti, A. Attractions and repulsions in molecular crystals: What can be learned from the crystal structures of condensed ring aromatic hydrocarbons? *Accounts Chem Res* **1999,** *32*, 677.

[65] Olsen, J.; Seiler, P.; Wagner, B.; Fischer, H.; Tschopp, T.; Obst-Sander, U.; Banner, D. W.; Kansy, M.;

Muller, K.; Diederich, F. A fluorine scan of the phenylamidinium needle of tricyclic thrombin inhibitors: effects of fluorine substitution on pKa and binding affinity and evidence for intermolecular C-F...CN interactions. *Org Biomol Chem* **2004,** *2*, 1339.

[66] Asai, T.; Tsuzuku, T.; Takahashi, S.; Okamoto, A.; Dewa, T.; Nango, M.; Hyodo, K.; Ishihara, H.; Kikuchi, H.; Oku, N. Cell-penetrating peptide-conjugated lipid nanoparticles for siRNA delivery. *Biochemical and biophysical research communications* **2014,** *444*, 599.

[67] Yamakawa, S.; Furuyama, Y.; Oku, N. Development of a Simple Cell Invasion Assay System. *Biol Pharm Bull* **2000,** *23*, 1264.

[68] Koide, H.; Okamoto, A.; Tsuchida, H.; Ando, H.; Ariizumi, S.; Kiyokawa, C.; Hashimoto, M.; Asai, T.; Dewa, T.; Oku, N. One-step encapsulation of siRNA between lipid-layers of multi-layer polycation liposomes by lipoplex freeze-thawing. *Journal of controlled release* **2016,** *228*, 1.

[69] Bailey, A. L.; Cullis, P. R. Modulation of membrane fusion by asymmetric transbilayer distributions of amino lipids. *Biochemistry* **1994,** *33*, 12573.

[70] Tai, W.; Gao, X. Functional peptides for siRNA delivery. *Adv Drug Deliv Rev* **2017,** *110*, 157.

[71] Sahay, G.; Querbes, W.; Alabi, C.; Eltoukhy, A.; Sarkar, S.; Zurenko, C.; Karagiannis, E.; Love, K.; Chen, D.; Zoncu, R.; Buganim, Y.; Schroeder, A.; Langer, R.; Anderson, D. G. Efficiency of siRNA delivery by lipid nanoparticles is limited by endocytic recycling. *Nature biotechnology* **2013,** *31*, 653.

[72] Evans, W. H.; Hardison, W. G. Phospholipid, cholesterol, polypeptide and glycoprotein composition of hepatic endosome subfractions. *Biochem J* **1985,** *232*, 33.

[73] Huotari, J.; Helenius, A. Endosome maturation. *EMBO J* **2011,** *30*, 3481.

[74] Light, W. G.; Wei, E. T. Surface charge and hemolytic activity of asbestos. *Environ Res* **1977,** *13*, 135.

[75] Stalder, L.; Heusermann, W.; Sokol, L.; Trojer, D.; Wirz, J.; Hean, J.; Fritzsche, A.; Aeschimann, F.; Pfanzagl, V.; Basselet, P.; Weiler, J.; Hintersteiner, M.; Morrissey, D. V.; Meisner-Kober, N. C. The rough endoplasmatic reticulum is a central nucleation site of siRNA-mediated RNA silencing. *EMBO J* **2013,** *32*, 1115.